STUDIES ON TECHNIQUES FOR SATELLITE SURVEILLANCE OF GLOBAL ATMOSPHERIC POLLUTION

by

Michael McClintock
T. A. Hariharan
Alden McLellan IV

A Report to

THE NATIONAL AIR POLLUTION CONTROL ADMINISTRATION

on Research Conducted Between
September 1, 1969 and July 31, 1970

(Contract Period July 1, 1969 to September 30, 1970)

Contract No. CPA 22-69-101

Principal Investigator: Verner E. Suomi

The Space Science and Engineering Center
The University of Wisconsin
1225 West Dayton Street
Madison, Wisconsin 53706

September 30, 1970

STUDIES ON TECHNIQUES FOR SATELLITE SURVEILLANCE OF GLOBAL ATMOSPHERIC POLLUTION

by

Michael McClintock
T. A. Hariharan
Alden McLellan IV

A Report to

THE NATIONAL AIR POLLUTION CONTROL ADMINISTRATION

on Research Conducted Between
September 1, 1969 and July 31, 1970

(Contract Period July 1, 1969 to September 30, 1970)

Contract No. CPA 22-69-101

Principal Investigator: Verner E. Suomi

The Space Science and Engineering Center
The University of Wisconsin
1225 West Dayton Street
Madison, Wisconsin 53706

September 30, 1970

CONTENTS

SUMMARY

This report to the National Air Pollution Control Administration covers research on the feasibility of using satellites to study air pollution. It is not an exhaustive analysis of the many ways in which satellites might be used for such studies. Rather, since it was established somewhat quickly that satellites appear to have much to offer for certain measurements which are needed immediately, we have made an initial survey of several areas that look especially promising.

The chapter on Remote Sensing of Particulates in the Atmosphere stresses the information about aerosols that is obtainable from polarization measurements. Turbidity from Sun-glitter Observations deals with what we believe to be a new experimental technique: the possibility of "calibrating" the intensity of specularly reflected sunlight and using this optical source to measure the spectral turbidity of the atmosphere. Turbidity from ATS Measurements illustrates the use of existing ATS data to obtain information about atmospheric turbidity over the Los Angeles basin. Techniques for Remote Sensing of Gaseous Air Pollutants is a review of the available spectroscopic methods that appear most promising for possible satellite use. Measurement of CO from SMS Satellite is an outline for an experimental measurement of atmospheric CO that involves a minor modification to an existing satellite plan. Application of Lasers to Air Pollution Research reviews a selection of ways in which lasers have been or are likely to be applied to air pollution studies.

None of the above topics, with the exception of the ATS measurements, has been taken beyond the concept stage to proper quantitative evaluation. The conclusions we draw from this initial survey, therefore, must be considered tentative. But within this context we conclude that the most promising subjects to pursue further for more quantitative evaluation at present are two particular

experiments designed to measure the variation of albedo and of atmospheric turbidity in the spectral regions important to the radiative energy balance of the planet.

The reasoning is as follows: the spectral advantage of satellite-based experiments is their ability to provide global coverage, and they can do this at a lower cost than a network of attended ground stations. Indeed, certain quantities, for example global albedo, can be measured with precision in no other way. Among the air-pollution problems characterized by global scope, the possibility of climatic change caused by changes in the atmospheric composition is of prime importance. The correlation between climate and mean temperature that is thought to exist, therefore, suggests that instrumentation should be developed to measure the quantities appropriate to the terrestrial energy balance. Furthermore, particular attention must be paid to the variation with time of these quantities. After all, it is the prospect of climatic change we should be concerned about rather than climate itself, since present life has a strong bias toward the environment in which it has evolved.

The quantities most pertinent to the energy balance are the atmospheric turbidity and planetary albedo, and these quantities can also be measured with greater precision than they can be calculated using indirect methods. For example, from knowledge of the particulate content of the atmosphere, one must solve the radiative transfer problem to some suitable approximation using Mie scattering theory in order to arrive at the radiant energy transmitted through the atmosphere. The more direct approach is merely to measure the radiation in the important spectral regions which is transmitted (turbidity) and that which is backscattered (albedo). Not only are the complexities of the Mie theory avoided, but also its approximations, so the resulting energy balance is more precisely determined.

Of course, this approach allows one to obtain only limited detailed information about particulates, so other approaches may be called for in the future; but given the importance of the planetary energy balance, it would seem wise

to adopt the most direct and most precise experimental route to the solution of this problem. We therefore conclude the feasibility studies of measuring turbidity and albedo should be pursued vigorously in the coming year.

One of the initial efforts in this last period has been directed at an attempt to detect air pollution in the Los Angeles basin from existing ATS-III data. Here we have tried to capitalize on an opportunity that has presented itself, and the results indicate promise, although they must be carried a bit further to be made satisfactorily quantitative.

The place of satellites in air-pollution research, as distinct from monitoring, can be illustrated by the problem of carbon monoxide. If an experiment can be devised to measure CO content in the various regions of the globe, this knowledge may well help to answer the question of what constitute the major sinks for this molecular pollutant. Certainly the atmospheric history of CO must eventually be understood in order to provide guides for allowable production of this gas from the global point of concern. Barring the possibility of an early experiment aboard a SMS satellite, however, we prefer to invest our resources in the problems already mentioned.

Conclusions drawn from the other topics in this report would be premature. There is certainly a place for lasers in air-pollution research, for example, but our feeling at present is that they will be most helpful in the solution of air-pollution problems on local and regional scales, with special applications to remote techniques, but that better sources exist for satellite-based experiments. In particular, the sun. Given the usefulness of this intense, wide-band spectral source, one must reflect cautiously before electing to pay the price in terms of weight, power requirements and reliability that would be necessary to fly a laser. More definitive conclusions are reserved for the future.

I. GLOBAL AIR POLLUTION

Two Scales of the Problem

The major impetus for concern about air pollution in recent years has come from the problems observable on a local scale. Near the major sources, given certain local geographic and atmospheric conditions, air pollution often reaches palpable proportions. Even if one denies the biological effects of air pollution in these regions, there is clearly a strong aesthetic motivation to attempt its abatement. A very broad spectrum of activity is therefore currently directed toward developing the necessary measurement techniques and working out the proper control programs to reclaim this aspect of the local environment.

But the problem of air pollution exists on a global scale as well. Here, however, the reasons for concern are quite different. Although the concentration of carbon monoxide in certain local environments, for example, has been measured at over 100 parts per million at times, levels which are considerably toxic to human life, one is not concerned that global concentrations will reach toxic levels. Long before that has occurred, local levels will become intolerable and corrective efforts will become mandatory.

Carbon monoxide has a place in a global study, but not for reasons of toxicity. A measurement of the world-wide distribution of CO provides information about its life history. The mean atmospheric lifetime can be obtained from such measurements, a quantity important to allow the establishment of acceptable rates of production of CO by combustion processes. Furthermore, since virtually all of the atmospheric CO is thought to be manmade, a study of its life history will provide important information about the dynamics of pollution.

To take another example, the increase of carbon dioxide in the atmosphere has an effect on the radiation balance of the planet, and hence on its mean

temperature. But because it is transparent and non-toxic, carbon dioxide is not considered a pollutant on the local scale. From a global point of view, however, its indirect effect on climate forces its consideration as an atmospheric pollutant.

Thus we see the existence of two sets of problems arising from pollution of the atmosphere, one set on the local or regional scale, and another set, not homomorphic with the first, on the global scale. The appropriate place of satellite-based instrumentation to investigate problems of the second kind, global problems, is not difficult to establish. What may not be thoroughly appreciated, however, is its appropriateness for certain problems of more limited geographical extent. The present report deals with initial feasibility studies of some problems of both kinds.

Problems of a Changing Atmosphere

The atmosphere of the Earth has always been changing, of course. From an early atmosphere that was predominantly reducing, there has been evolution to the present composition in which oxygen is one of the major constituents and supports the animate life forms that have evolved along with the changing atmosphere. Berkner and Marshall [1], and more recently, Johnson [2] have documented certain major aspects of this atmospheric evolution. Furthermore, the evolution of the forms of life that exist on Earth has taken place in the past on the geologic time scales that characterize the changing atmosphere. This is so, of course, because viable life forms either changed in ways compatible with support by the changing environment, or they became extinct.

Recently, however, an important new element has entered the picture. Man has become so populous and sophisticated technologically that his own activities are now changing the composition of the atmosphere in addition to the natural causes. But since the time scales on which man's activities are changing the atmosphere are much smaller than geologic time scales, there is need to be concerned. Changes of sufficient magnitude may render the Earth uninhabitable

by life forms we know, and if the changes occur in a time that is short compared to the time necessary for evolution to accommodate to them, life may become extinct. This could happen, for example, if there are gross instabilities in the atmospheric composition, triggered by the smaller changes which man causes by his pollution; or it could happen if there are gross instabilities in climate, again triggered by changes in the atmosphere. No satisfactory working model exists at present of the complex atmospheric system, let alone its interaction with other elements to produce climatic change, so it is impossible to say. But geologic documentation of past ice ages standa as irrefutable evidence that climatic instabilities have existed in the past. Their improbability is not sufficient reason for neglecting to attempt an understanding of the causes.

But even if one denies the importance of understanding large-scale cataclysmic phenomena, interest in atmospheric change of less serious consequence is provided by our strong bias toward the world as we know it now—toward what we call a natural environment, even though it is only remotely related to natural environments that have existed in the past, and even though it is almost certain to be changed somewhat in the future. We exist at a precise moment in the geologic history of the Earth, and it should not be surprising that our immediate experience with the environment that also exists at the same moment provides us with this bias. It makes sense, therefore, for us to address ourselves to those problems that will be presented by the changes now taking place in the Earth's atmosphere, if we are clever enough to figure out what they are. We seek an understanding of the cause-and-effect relationships that lead to these problems. The hope is that, as in the many other cases which provide precedent, the proper measurements, properly made, will help lead to such understanding. The further hope is that adequate understanding of their causes will suggest solutions.

II. REMOTE SENSING OF PARTICULATES IN THE ATMOSPHERE

General Characteristics of Particulates

The nature of air pollution resulting from particulates is significantly different from that produced by gases. When particulates have a very small diameter, generally less than 20 microns for materials of common density, they exhibit transport properties similar to gases. Their free settling velocities are so low that they have motions in the atmosphere approximated by the surrounding gases.

A number of distinct effects are produced by particles, the important ones being visibility reduction, changes in electrical conductivity, formation of fogs, possible increase in the albedo of the earth and biological effects via respiratory infection. Aerosols are also known to react with gaseous pollutants to form complex substances which are potentially more hazardous as pollutants, compared to the individual components.

Atmospheric aerosol particles form a heterogeneous population with respect to size, morphology, electrical properties, composition and concentration. The aerosol is in a dynamic state of change as a result of the physical and chemical properties of both the particles and the atmosphere.

Particulates in the atmosphere spring from a wide range of sources. Those larger than 10 microns in diameter come mainly from mechanical processes such as erosion, grinding and spraying. Those between 10 and 1 microns are more numerous in the atmosphere and generally include the largest weight fraction of particles. They also stem from mechanical processes and include industrial dusts, ash and the like. Particles in the size range between 0.1 and 1 micron tend to contain more of the products of condensation than do larger particles. The products of combusion along with aerosols formed by photochemical

reactions predominate in this range. Very little is known of the chemical nature of particles in the size range below 0.1 micron. Over cities their concentration is characteristically higher than the rural level and the difference seems to be due largely to combustion.

Particles of all kinds and sizes share a number of physical properties. They grow by condensation, adsorb and absorb vapors and gases, coagulate or disperse, and absorb or scatter light. It is not possible to generalize on the chemical behavior of particles because they are so diverse and because so little is known of them.

Gravitational settling is the main mechanism by which particles are removed ultimately from the air, but there are intervening mechanisms that vary with the size of the particle. Particles that are less than 0.1 micron in diameter move randomly in air, collide often with other particles and grow rapidly by coagulation. Particles in this size range would soon vanish from the air were they not replenished constantly by these condensation processes. Particles in the next larger size range, 0.1 to 1.0 micron, probably are also removed from the air by coagulation. They grow more slowly than the smaller particles. At diameters larger than 1 micron, particles begin to develop appreciable settling velocities, and above 10 microns they begin to settle relatively rapidly, although particles as large as 10 microns can be kept airborne by turbulence for extended periods.

Particles may be removed from the air by impinging on buildings, trees and other objects. Rain also removes them, but the effect is negligible at particle diameters of less than 2 microns. The processes that remove particles from the air combined with the steady generation of small particles by condensation and of large particles by mechanical processes tend to cause particulate matter to maintain a relatively constant size distribution in air. This distribution covers a range of diameters of about 0.001 micron to a few tens of microns. Particles in the range 0.1 to 10 microns account for most of the mass and a large fraction of the number present.

Particles generated in an urban atmosphere normally remain airborne for

only a few days although depending on their size they may remain airborne for several weeks. Gravitational settling prevents larger particles such as fly ash from travelling very far from their sources. The lifetime of a particle in air is a strong function of the height at which it is introduced. However, large or intense sources such as big metropolitan areas, erupting volcanos, nuclear explosions, and forest fires can produce particles that travel around the world.

Measurements of the concentration of airborne particles at remote points are scanty but there are indications that the global level is rising. These indications include measurements of both atmospheric turbidity and the electrical conductivity of the air. Particles in the air scatter incoming sunlight, reducing the amount that reaches the earth and thus tend to lower the temperature of the surface. There is justifiable concern that particulate matter generated by man and other natural causes could be contributing to important geophysical phenomena. Continuous monitoring of the concentration of the particulate matter to a high precision is an ambitious program at this stage, considering the present state of the art in remote sensing techniques for particulates. (The status of atmospheric turbidity measurements, however, is another matter, and this is considered later.)

Theory of Light Scattering by Aerosols

Almost all the remote sensing techniques presently applied or conceived make use of the nature of interaction of the particles with the electromagnetic radiation incident on them either from the natural source, i.e. the sun, or artificial sources like searchlights and lasers. Before evaluating the experimental methods a brief account is given of the main features of the interaction and the physical principles involved. An assumption, not completely justified, is often made that the absorption by particulates in the visible part of the spectrum is negligible. What is most important is the scattering characteristics formulated by Mie and the resulting attenuation of radiation passing through a medium containing particulates.

In the case of molecules and very small particles whose radii, r, satisfy the relation

$$2\pi r << \lambda \tag{1}$$

where λ is the wavelength of the incident radiation, the scattering is described by the well known Rayleigh theory. The Rayleigh scattering coefficient, σ_R, at altitude h above ground level may be written as

$$\sigma_R(\lambda) = 10^5 \frac{32\pi^3}{3} \frac{(m_\lambda - 1)^2}{\lambda^4} \frac{N(h)}{N_0^2} \frac{6 + 3\Delta}{6 - 7\Delta} \tag{2}$$

where m_λ = index of refraction of air at ground level (15°C and 1013 mb pressure for standard atmosphere)

$N(h)$ = molecular number density as a function of height h

N_0 = $N(h)$ at ground level

Δ = depolarization factor

The scattering coefficient has the dimensions of length^{-1}, and is equal to the scattering cross section per particle times the number of scatterers per unit volume.

The angular distribution of light scattered by molecules is defined by the ratio of the radiance scattered by a unit volume of molecules at the angle ϕ to the total irradiance incident upon the volume element

$$F_R(\phi, \lambda) = \frac{3}{16\pi} \sigma_R(\lambda)(1 + \cos^2 \phi) \qquad [\text{km}^{-1}\ \text{sr}^{-1}] . \tag{3}$$

The index of refraction, m_λ, for a standard atmosphere is given by Edlen's formula [3]

$$(m_\lambda - 1) \times 10^8 = 6432 \cdot 8 + \frac{2949810}{146 - (\lambda^{-2})} + \frac{25540}{41 - (\lambda^{-2})} \tag{4}$$

with λ in microns.

The spectral attenuation of radiation due to scattering and absorption while traversing an optically thin homogeneous medium is expressed as

$$I(\lambda) = I_0(\lambda) e^{-\sigma_E(\lambda) L} \tag{5}$$

The quantity $\sigma_E(\lambda)$ (km^{-1}) defines the extinction coefficient.

In the visible region the extinction coefficient is given as the sum of the molecular (Rayleigh) scattering coefficient σ_R, the aerosol-attenuation coefficient σ_A, and the ozone absorption $\sigma_0(\lambda)$. The effect of other molecular constituents is neglected. The ozone absorption is quite small and also is often neglected.

The scattering of light by aerosols is expressed by the Mie theory considering a spherical shape for the particles and assuming they are non-absorbing. When unpolarized light of intensity I_0 and wavelength λ propagates in the region of a sphere of homogeneous material of radius r and refractive index m, the scattered radiation field has two intensity functions, i_1 and i_2, polarized normal and parallel to the plane of observation, respectively, and the total intensity per steradian scattered into a direction at an angle ϕ to the incident direction is given by [4]

$$I = \frac{\lambda^2}{4\pi^2 R^2} \frac{i_1 + i_2}{2} I_0 \tag{6}$$

where R is the distance from the sphere. The size of the sphere is generally determined by the dimensionless parameter

$$x = \frac{2\pi r}{\lambda} . \tag{7}$$

The intensity functions i_1 and i_2 are functions of the scattering angle ϕ and may be interpreted as the squares of the amplitude functions S_1 and S_2:

$$i_1 = |S_1|^2 \qquad i_2 = |S_2|^2 \tag{8}$$

with

$$S_1(r, \lambda, m, \phi) = \sum_{n=1}^{\infty} \frac{2n+1}{n(n+1)} [a_n \pi_n + b_n \tau_n] \tag{9}$$

and

$$S_2(r, \lambda, m, \phi) = \sum_{n=1}^{\infty} \frac{2n+1}{n(n+1)} [a_n \tau_n + b_n \pi_n] . \tag{10}$$

The Mie coefficients a_n and b_n may be written in the form [5]

$$a_n = \frac{\psi_n'(mx)\psi_n(x) - m\psi_n(mx)\psi_n'(x)}{\psi_n'(mx)\xi_n(x) - m\psi_n(mx)\xi_n'(x)} \tag{11}$$

$$b_n = \frac{m\psi_n'(mx)\psi_n(x) - \psi_n(mx)\psi_n'(x)}{m\psi_n'(mx)\xi_n(x) - \psi_n(mx)\xi_n'(x)} \tag{12}$$

with

$$\psi_n(x) = xJ_n(x) \quad ; \quad \xi_n(x) = xH_n^{(2)}(x) \tag{13}$$

where $J_n(x)$ are spherical Bessel functions and $H_n^{(2)}(x)$ are the spherical Hankel functions of the second kind. The primes indicate differentiation with respect to the argument. m is the index of refraction of the particle. The angle dependent π_n and τ_n are the first and second derivatives of the Legendre polynomials $P_n(\cos\phi)$ of order n and argument $\cos\phi$.

$$\pi_n = \frac{dP_n(\cos\phi)}{d\cos\phi} \tag{14}$$

$$\tau_n = \cos\phi\,\pi_n - \sin\phi\,\frac{d\pi_n}{d\cos\phi} \quad . \tag{15}$$

The scattering cross section C_{sc} and the efficiency factor Q_{sc} may be calculated from the series

$$C_{sc}(\lambda, r, m) = \frac{\lambda^2}{2\pi}\sum_{n=1}^{\infty}(2n+1)(|a_n|^2 + |b_n|^2) \tag{16}$$

$$Q_{sc}(x, m) = \frac{C_{sc}(\lambda, r, m)}{\pi r^2} = \frac{2}{x^2}\sum_{n=1}^{\infty}(2n+1)(|a_n|^2 + |b_n|^2) \, . \tag{17}$$

The scattering efficiency factor Q_{sc} can be computed for assumed values of m and x and a typical result [6] for $m = 1.5$ and $x = 0.193$ to 139.6 is shown in Fig. 1.

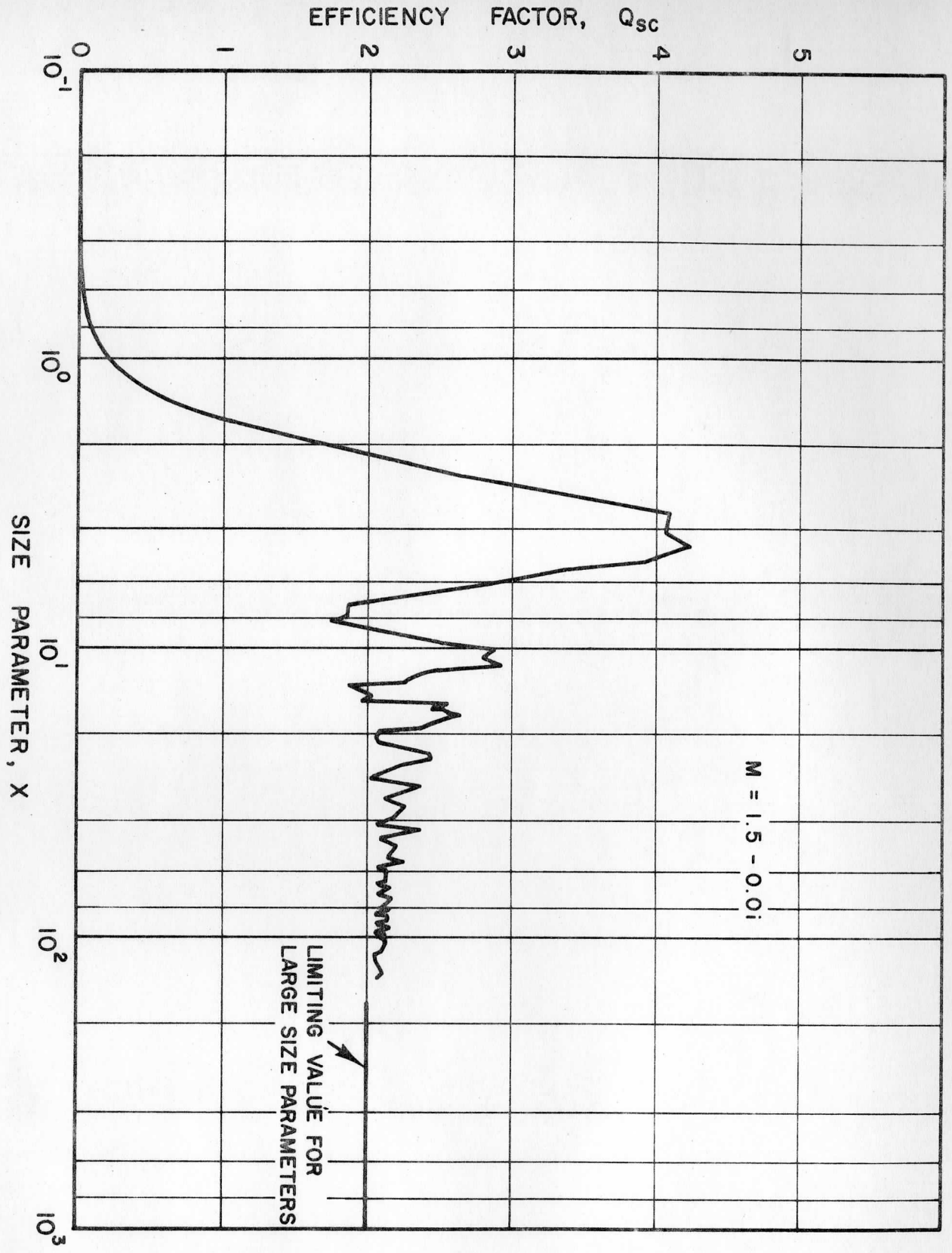

Fig. 1. Scattering Efficiency for Size Parameters Greater than X = 0.2 (Blättner)

When considering the scattering function and the scattering coefficient of a unit volume of air, it is necessary to integrate the microscopic Mie scattering data over the aerosol-size distribution.

In a medium containing N particles per cm^3 with the size distribution n(r) particles per cm^3 and per radius interval

$$N = \int_{r_1}^{r_2} n(r)dr \tag{18}$$

where r_1 and r_2 are the minimum and maximum radii in the particle distribution. The total scattering coefficient of all particles with the radius $r = R$ is given by

$$\sigma_{sc}(m, \lambda) = C_{sc}(m, r, \lambda)n(R) \ . \tag{19}$$

The total scattering coefficient for a distribution of sizes is

$$\sigma_{sc}(m, \lambda) = \int_{r_1}^{r_2} C_{sc}(m, \lambda, r)n(r)dr \quad [km^{-1}] \ . \tag{20}$$

The macroscopic scattering function

$$f(\phi, \lambda) = \int_{r_1}^{r_2} F(\phi, r/\lambda)n(r)dr \tag{21}$$

$$f(\phi, \lambda) = \int_{r_1}^{r_2} \frac{r^2}{x^2} \frac{i_1 + i_2}{2} n(r)dr$$

$$= \frac{\lambda^2}{4\pi^2} \int_{r_1}^{r_2} \frac{i_1 + i_2}{2} n(r)dr \ . \tag{22}$$

The scattering function may be interpreted as the intensity per steradian of radiation of wavelength λ being scattered in the direction of ϕ per unit amount of radiation incident on the volume element. The integration of $f(\phi, \lambda)$ over 4π solid angle is therefore equivalent to the total scattered intensity per unit length of scattering volume, i.e., the scattering coefficient

$$\sigma_{sc}(\lambda) = 2\pi \int_0^{\pi} f(\phi, \lambda) \sin \phi \, d\phi \tag{23}$$

The optical effect of aerosols in the atmosphere depends on a number of factors such as their physical structure, chemical composition (index of refraction), size distribution and concentration. Since not all these parameters are known, model atmospheres with restrictive assumptions have to be considered. It is generally assumed that the aerosols are homogeneous spheres. Indirect determinations of the index of refraction result in values consistent with the assumptions, which indicates that the index of refraction may be described by a value between 1.50 to 1.55 for the real part, and a very small value, < 0.01, for the imaginary part. The first systematic measurements [7] show that the size distribution may be approximated over a large range of particle radii by a power law as follows:

$$\frac{dN}{d \log r} = c\, r^{-\nu^*}$$

or

$$\frac{dN}{dr} = n(r) = c'\, r^{-(\nu^*+1)} \tag{24}$$

where ν^* has values between 2.5 and 4.0 with an average of 3.0.

Transmission of Radiation through a Turbid Atmosphere

For horizontal transmission T_h over a path L at any altitude h and extinction coefficient $\sigma_E(h, \lambda)$

$$T_h = \exp - \sigma_E(h, \lambda)\, L \tag{25}$$

For vertical and slant path transmission from sea level to a given altitude at zenith angle θ for all wavelengths of interest

$$T_{0-h} \doteq \exp[- \tau_{ext}(h) \sec \theta] \tag{26}$$

where

$$\tau_{exp}(h) = \int_0^{\infty} \int_0^{L} \sigma_E(h, \lambda) d\ell \, d\lambda \tag{27}$$

For vertical and slant path transmission between two altitudes above sea level

$$T_{\Delta h} = \exp - [\tau_{ext}(h_2) - \tau_{ext}(h_1)] \sec \theta \tag{28}$$

For vertical and slant path transmission from a given altitude out into space

$$T_{h-\infty} = \exp[- \tau'_{ext}(h) \sec \theta] . \tag{29}$$

These relations indicate that from a knowledge of the transmission of radiation from a source of known intensity it is possible to get information about the scattering parameters.

If the intensity of the direct solar radiation is measured at ground level at a number of spectral intervals it is possible not only to get information about the aerosol content or the level or turbidity but also the size distribution of the particles which cause the turbidity. If the attenuation of the radiation is expressed by the equation

$$I_\lambda = I_{0\lambda} e^{-a_\lambda M} \tag{30}$$

where I_λ is the spectral intensity of the direct solar radiation at ground level and of wavelength λ, $I_{0\lambda}$ is the extraterrestrial intensity of the sun, M is the relative air mass (at zenith $M = 1$) and a_λ the extinction coefficient. The extinction coefficient for the aerosols of the entire atmosphere is given by

$$a_{D\lambda} = \frac{\ell n\, I_{0\lambda} - \ell n\, I_\lambda}{M} - a_{R\lambda} \tag{31}$$

where $a_{R\lambda}$ is the extinction coefficient for molecular scattering according to Rayleigh theory. In order to calculate the size distribution from the observed wavelength dependence of extinction coefficients the equation

$$a_{D\lambda} = \int_0^\infty Q_{ext}\left(\frac{2\pi r}{\lambda}, m\right) \pi r^2 \frac{dN(r)}{dr}\, dr \tag{32}$$

has to be solved where $\frac{dN(r)}{dr}$ is the unknown size distribution.

The term Q_{ext} can be obtained from Mie theory. Using various aerosol size distributions and altering these distributions until reasonable agreement

is reached between the calculated extinction coefficients and the measured values, one can arrive at the most probable size distribution. This method has been successfully applied by Quenzel from measurements in eight spectral regions from $\lambda = 0.4$ to 1.6μ. A more direct inversiom method has been suggested by Yamamoto and Tanaka [8] which has many similarities to the inversion method applied to temperature sounding measurements.

The technique of determining turbidity from direct solar radiation measurements has been applied by several investigators [9-11]. The applicability of the method for satellite surveillance of global turbidity has to be based on the following considerations:

a) If extinction measurements are made through the limb of the earth, the time of observation will be limited to sunrise and sunset time.

b) Due to interference from clouds, low-level turbidity will be very difficult to measure. Most of the normal turbidity prevails in the lower atmosphere and hence measurements in this region are the most significant. However, dust layers are known to exist at higher altitude in the upper troposphere, extending into the stratosphere, and measurement of changes in the particulate concentration in these layers may have immense significance.

Turbidity from Diffuse Radiation Measurements

A different approach to measure turbidity on a global scale makes use of the diffusely reflected (scattered) solar radiation. Part of the radiation incident on the atmosphere is sent back to space after being scattered by the constituents, and a measurement of this radiation can give information about the scatterers and the level of turbidity.

The measurement of the intensity and polarization of skylight (diffusely transmitted radiation) has shown for a long time considerable deviation from the theoretical values for a molecular atmosphere. One reason for these deviations is the presence of particulates which cause haze turbidity. For purposes of global surveillance, these ground-based measurements are not as suitable

as the measurement from a satellite of the diffusely reflected radiation, which is the radiation leaving the earth after being scattered by all the constituents and reflected by underlying ground as well as clouds [12].

Earlier studies of atmospheric turbidity from measurements of skylight polarization were based on the degree of maximum polarization and the positions of the neutral points in the sun vertical (local meridian through the sun). For a pure molecular atmosphere, the measured quantities would depend only on the optical thickness and the nature of ground reflection. For large optical thicknesses the accuracy of the determination decreases and for optical thickness greater than one, the determination is not even unique. It is possible to modify the method of measurement as suggested by radiative transfer theory to arrive at better quantitative estimates of aerosol content.

If the particulate matter in the atmosphere scatters light according to the Mie theory, then the Stokes parameters for the upward radiation can be expressed in series form

$$I_\ell(0;\mu,\phi) = \sum_{n=0}^{N} I_\ell^{(n)}(\tau;\mu,\mu_0)\cos n(\phi-\phi_0) + I_\ell^* \tag{33}$$

$$I_r(0;\mu,\phi) = \sum_{n=0}^{N} I_r^{(n)}(\tau;\mu,\mu_0)\cos n(\phi-\phi_0) + I_r^* \tag{34}$$

$$U(0;\mu,\phi) = \sum_{n=0}^{N} U^{(n)}(\tau;\mu,\mu_0)\sin n(\phi-\phi_0) + U^* \tag{35}$$

where the symbols have the usual meaning as applied to radiative transfer theory [13]. The inversion problem is reduced to the determination of τ and ground reflectivity from the values of I_ℓ, I_r, U, I_ℓ^*, I_r^*, and U^*.

For Rayleigh scattering, we have from the theory of radiative transfer $N = 2$ and the following relations hold between the coefficients

$$I_r^{(1)} = U^{(0)} = 0$$

$$I_\ell^{(1)} = \mu U^{(1)} \tag{36}$$

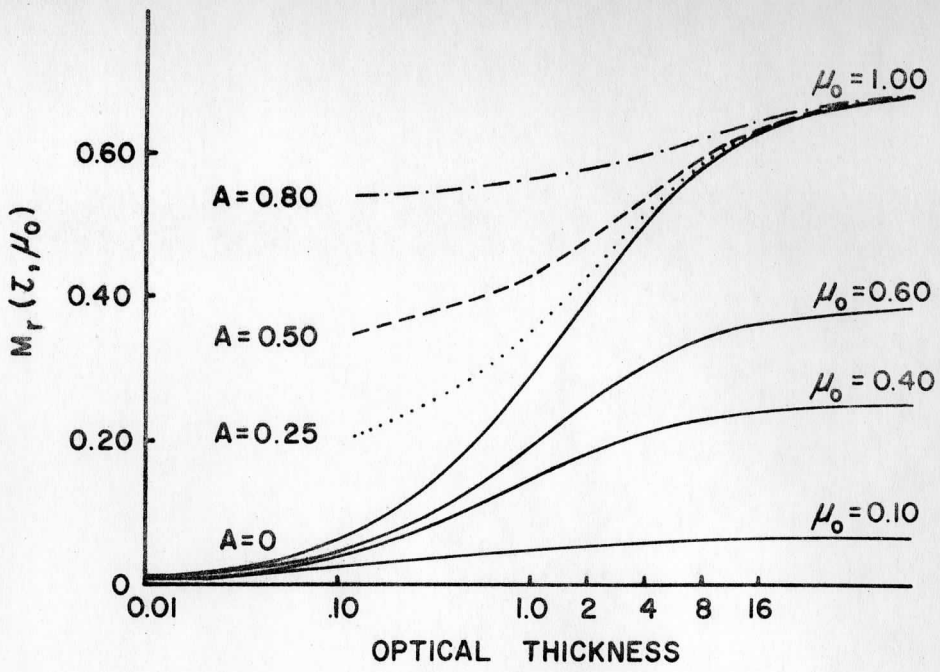
$M_r(\tau,\mu_0)$
0.60
0.40
0.20
0
A=0.80
A=0.50
A=0.25
A=0
$\mu_0=1.00$
$\mu_0=0.60$
$\mu_0=0.40$
$\mu_0=0.10$
0.01
.10
1.0
2
4
8
16
OPTICAL THICKNESS

Fig. 2.

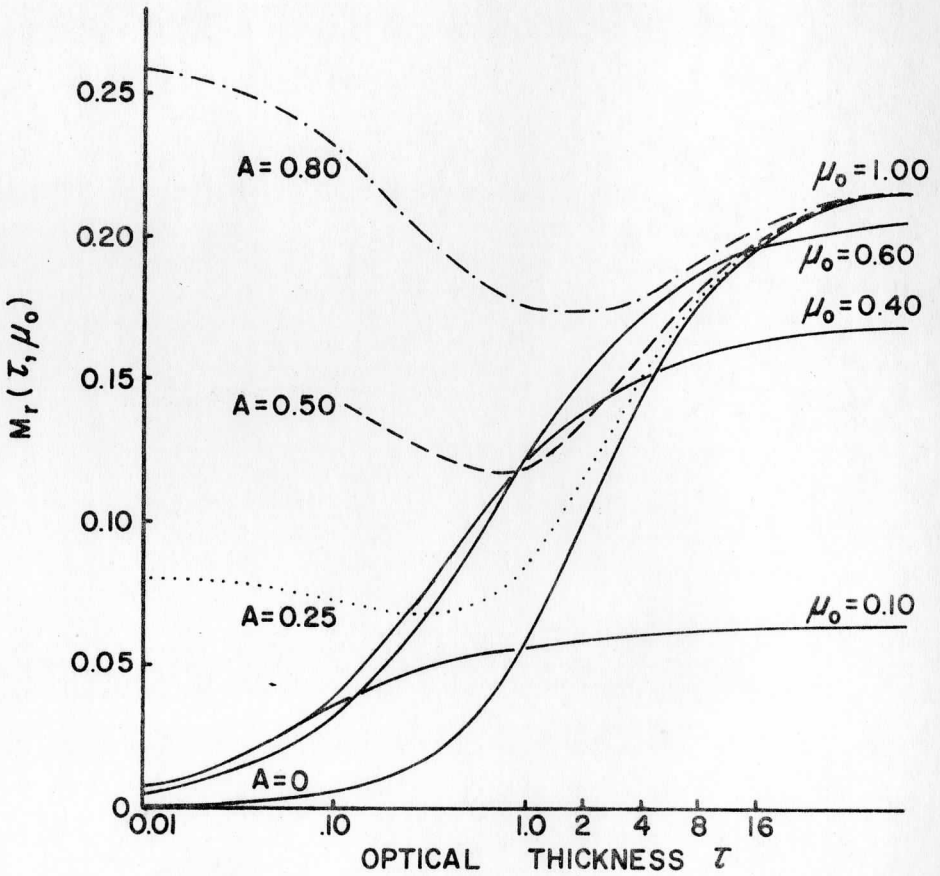
$M_r(\tau,\mu_0)$
0.25
0.20
0.15
0.10
0.05
0
A=0.80
A=0.50
A=0.25
A=0
$\mu_0=1.00$
$\mu_0=0.60$
$\mu_0=0.40$
$\mu_0=0.10$
0.01
.10
1.0
2
4
8
16
OPTICAL THICKNESS τ

Fig. 3.

$$I_\ell^{(2)} = -\mu^2 I_r^{(2)} = \frac{1}{2}\mu U^{(2)}$$

Because of these relations, there remain only four coefficients for use in inversion: $I_\ell^0(\tau, \mu, \mu_0)$, $I_r^0(\tau, \mu, \mu_0)$, $I_\ell^2(\tau, \mu, \mu_0)$ and $U^1(\tau;\mu, \mu_0)$, writing

$$I^{(0)} = \begin{bmatrix} I_\ell^{(0)} \\ I_r^{(0)} \end{bmatrix} \tag{37}$$

and reducing the equation for I^0 from radiative transfer theory we can arrive, after some simple mathematical manipulations, at the following relations

$$m_2[I_\ell^{(0)}(\tau,\mu)] + m_0[I_r^{(0)}(\tau, \mu)] = F_0 M_\ell(\tau, \mu_0) \tag{38}$$

$$m_0[I_\ell^{(0)}(\tau, \mu)] - m_2[I_\ell^{(0)}(\tau, \mu)] = F_0 M_r(\tau, \mu_0) \tag{39}$$

where

$$m_n[F(\mu)] = \int_0^1 F(\mu)\mu^n d\mu \tag{40}$$

The functions on the right-hand side of Equations 38 and 39 are known functions of the optical thickness and μ_0. The values of the functions $M_\ell(\tau, \mu_0)$ and $M_r(\tau, \mu_0)$ are plotted in Figs. 2 and 3 as functions of the optical thickness τ for several values of the parameter μ_0.

Similarly, $U^{(1)}(\tau, \mu, \mu_0)$ and $I_r^{(2)}(\tau, \mu, \mu_0)$ lead to the following relations:

$$\int_0^1 (1-\mu^2)^{1/2}(1+2\mu^2)U^{(1)}(\tau, \mu, \mu_0)d\mu = F_0 M^{(1)}(\tau, \mu_0) \tag{41}$$

and

$$\int_0^1 (1+\mu^2)^2 I_r^{(2)}(\tau, \mu, \mu_0)d\mu = F_0 M^{(2)}(\tau, \mu_0) . \tag{42}$$

The functions $M^1(\tau\mu_0)$ and $M^2(\tau\mu_0)$ are plotted in Figs. 4 and 5 as functions of τ for various values of μ_0.

Substituting the measured values (expressed in units of F_0) of the coefficients $I_\ell^{(0)}$, $I_r^{(0)}$, $U^{(1)}$ and $I_r^{(2)}$, we obtain the values of $M_\ell(\tau\mu_0)$,

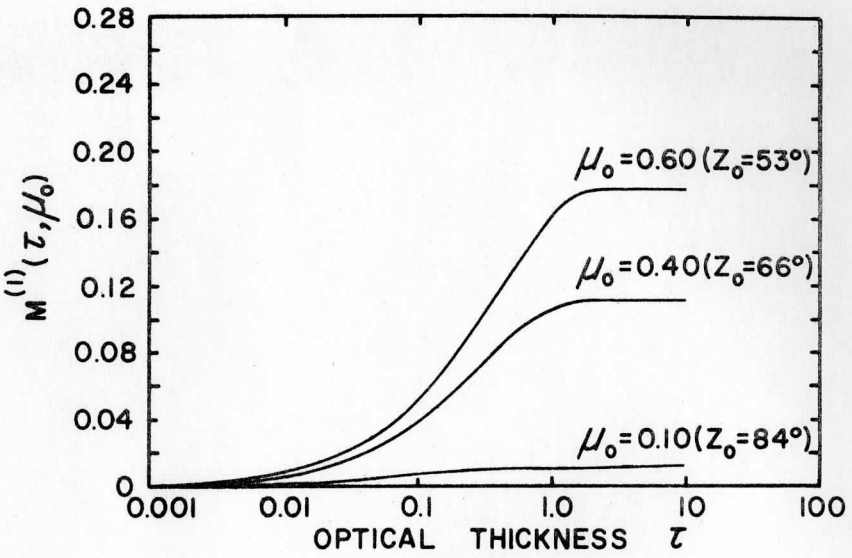
0.28
0.24
0.20
0.16
0.12
0.08
0.04
0
$M^{(1)}(\tau,\mu_0)$
$\mu_0=0.60(Z_0=53°)$
$\mu_0=0.40(Z_0=66°)$
$\mu_0=0.10(Z_0=84°)$
0.001
0.01
0.1
1.0
10
100
OPTICAL THICKNESS τ

Fig. 4.

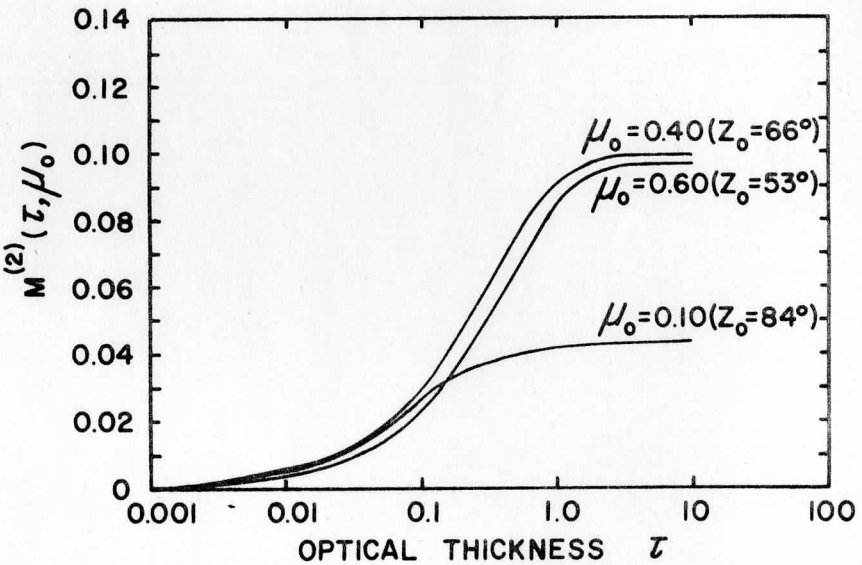
0.14
0.12
0.10
0.08
0.06
0.04
0.02
0
$M^{(2)}(\tau,\mu_0)$
$\mu_0=0.40(Z_0=66°)$
$\mu_0=0.60(Z_0=53°)$
$\mu_0=0.10(Z_0=84°)$
0.001
0.01
0.1
1.0
10
100
OPTICAL THICKNESS τ

Fig. 5.

$M_r(\tau\mu_0)$, $M^1(\tau\mu_0)$ and $M^2(\tau\mu_0)$.

From the diagrams we can obtain four independent estimates of the optical thickness.

For ground reflection according to Lambert's law with reflectivity A, only the functions M_ℓ^0 and M_r^0 are modified since the terms I_ℓ^* and I_r^* are azimuth independent and $U^* = 0$. After reducing the radiative transfer equations, we can arrive at the following relations:

$$m_2[I_\ell^{(0)}(\tau, \mu)] + m_0[I_r^{(0)}(\tau, \mu)] = F_0[M_\ell(\tau, \mu_0) + M_\ell^*(\tau, \mu_0; A)] \tag{43}$$

$$m_0[I_\ell^0(\tau, \mu)] - m_2[I_\ell^{(0)}(\tau, \mu)] = F_0[M_r(\tau, \mu_0) + M_r^*(\tau, \mu_0; A)]. \tag{44}$$

The variations of the functions $M_\ell(\tau\mu_0) + M_\ell^*(\tau, \mu_0; A)$ and $M_r(\tau, \mu_0) + M_r^*(\tau, \mu_0; A)$ with τ indicate that the monotonic increase of these functions disappears rapidly with increasing values of A. For larger values of A, we have to use only the functions $M^1(\tau, \mu_0)$ and $M^2(\tau, \mu_0)$ for the determination of the optical thickness. Figures 6 and 7 can be used for deriving the values of the ground reflectivity A. For Lambert's law and Rayleigh scattering the two values will be identical.

When the various conditions mentioned above are not satisfied, then there are two possibilities: either the ground reflection does not obey Lambert's law, or non-Rayleigh scattering is present in the atmosphere. The separation of these effects without additional information is a difficult problem.

To determine the general law of reflection it may be necessary to determine sixteen elements of the matrix defining the general law as functions of the direction of incident and reflected radiation.

The determination of non-Rayleigh scattering by particulates in the atmosphere is also difficult since the theory of radiative transfer in a turbid atmosphere is not fully solved.

The effect of aerosol scattering can be regarded as a perturbation of the

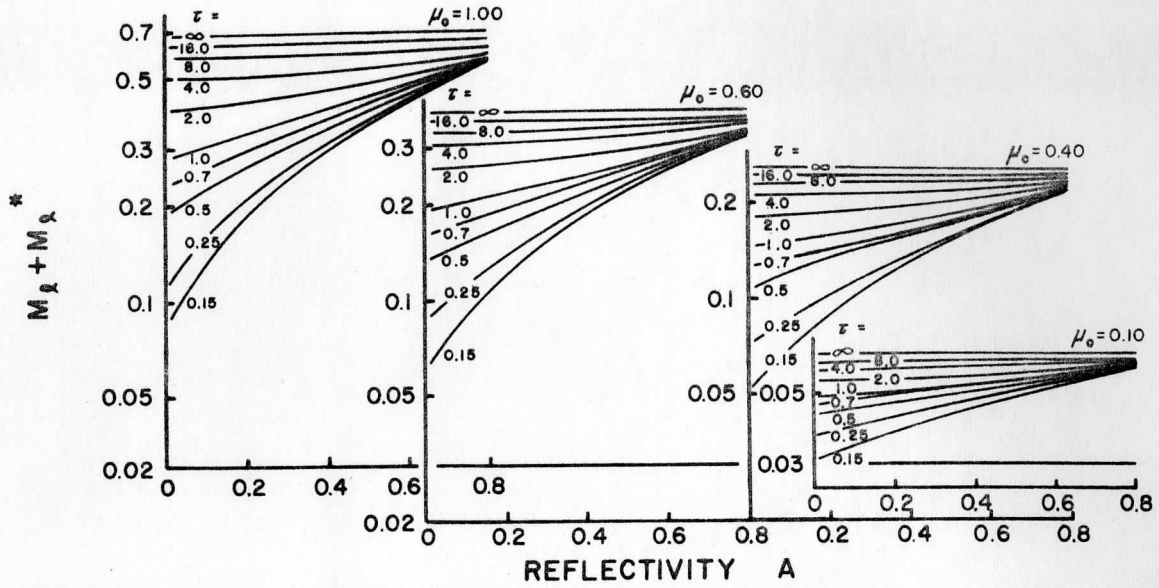
$M_q + M_q^*$
τ =
$\mu_0 = 1.00$
$\mu_0 = 0.60$
$\mu_0 = 0.40$
$\mu_0 = 0.10$
REFLECTIVITY A

Fig. 6.

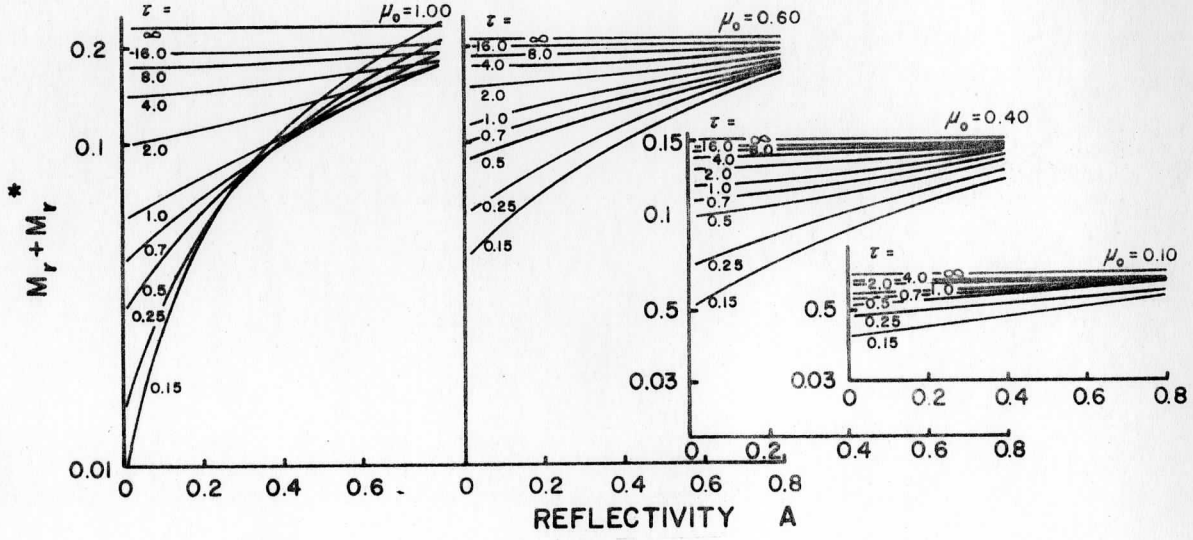
$M_r + M_r^*$
τ =
$\mu_0 = 1.00$
$\mu_0 = 0.60$
$\mu_0 = 0.40$
$\mu_0 = 0.10$
REFLECTIVITY A

Fig. 7.

polarization field of a pure molecular atmosphere. The coefficients I_ℓ^n, I_r^n, U^n can be computed for known values of τ_R and compared with the values derived from measurements. The effective parameters may then be determined from the differences between these values. The magnitude of the disagreement can be regarded as the first indication of the existence and magnitude of turbidity.

Essentially this theory shows that if measurements of the Stokes parameters of the upwelling radiation are made from a satellite-borne instrument and the values are compared with those theoretically computed for a molecular atmosphere, a first indication of the extent of atmospheric turbidity can be obtained from the difference between these values. Further information about the characteristics of the aerosols may be obtained by using models and curve fitting to account for the observed differences.

Some feasibility studies on the method of determination of atmospheric turbidity from polarization of the diffusely reflected radiation have been carried out using a photoelectric scanning polarimeter mounted on a high flying jet aircraft.[14] The measurements were made over various selected target areas of fairly uniform reflecting properties such as desert sand, clear ocean, farm lands, unbroken cloud decks, etc. From a comparison between the measured values of the degree of polarization of the diffusely reflected radiation and those computed for a purely molecular atmosphere [15] and a turbid atmosphere [16-19], some estimates of the turbidity could be derived after applying corrections for the uncertainty in the values of surface reflectance and the effect of multiple scattering in a turbid atmosphere. These results indicate that more systematic measurements of the three Stokes parameters and extensive comparisons with theoretically expected values would give more satisfactory and quantitative information on the level of turbidity. With a satellite-borne instrument the measurements can be made to cover the entire globe.

The corresponding radiative transfer theory for the diffusely transmitted radiation (skylight) has been worked out [20] and verified by experimental

observations. The measurement of the diffusely transmitted radiation is less suitable for global coverage, however, than satellite measurements.

The Very High Resolution Camera proposed for ATS provides for full earth coverage at a nadir resolution of 0.5 nm (0.025 mr). The instrument consists of a 10 in. aperture diameter Cassegranian telescope and a step drive mechanism to provide a 9600-line frame in 96 minutes or a modified 240-line in 24 minutes for the polarization experiment. The polarization experiment would require measurement of the intensity passed by polarizers oriented at four different angles, i.e., 0°, 45°, 90° and 135°, with respect to an arbitrary direction. Two or three spectral regions centered around 4500, 5500 and 6500Å can be conveniently covered. The results of a preliminary design study have already been made available to the Space Science and Engineering Center in the form of an unsolicited proposal by Santa Barbara Research Corporation. These studies should be pursued further to finalize the instrument parameters to make polarization measurements along with observation of clouds under very high resolution.

Solar Radiation Reflected from Artificial Satellites

Some artificial satellites have been designed with high reflectivity for solar radiation in the visible spectrum. Measurement of the radiation reaching the ground will give information about atmospheric effects such as attenuation due to aerosol scattering, absorption due to molecular constituents, etc. The instrumentation to be used will consist of a sensitive photometer with a high-power telescope foreoptics, the spectral regions of interest being controlled by appropriate filters. Calibration of the instrument can be made with standard type stars as the source of radiation. This calibration technique is applied in several astronomical observatories.

The technique of measuring ozone distribution in the atmosphere from observation of the reflected solar radiation from artificial satellites has been successfully applied by Venkateswaran, Moore and Kruger [21]. Similar measurements for turbidity and minor constituents are being attempted by Vanderburgh [22] at the Aerospace Research Laboratiries, USAF.

III. TURBIDITY FROM SUN-GLITTER OBSERVATIONS

The specular reflection of solar radiation from the ocean surface provides an intense source at the bottom of the atmosphere for observations from above. It seems possible to derive atmospheric turbidity and its spectral variations from measurements of the intensity of the sun-glitter. The feasibility of such an experiment, however, depends upon the ability to "calibrate" the intensity of this potentially useful spectral source each time a measurement is made, without resort to a complex system of ground-based instruments.

The various components of the radiation received by a satellite instrument are shown schematically in Fig. 8. Let R be the reflection coefficient and T, the fraction of radiation transmitted through the atmosphere in one passage. E_o is the sun's energy outside the earth's atmosphere; E_R is the sun's energy specularly reflected from the water surface and attenuated by two passes through the atmosphere; E_{Bo} is the black-body radiation at the surface of the earth, and E_B this radiation leaving the atmosphere; E_A is the energy scattered into the detector from the atmosphere and E_S that scattered from surface anomalies such as waves. Let S be the atmospheric scattering function appropriate to the geometry.

Consider first the region of the atmospheric window around 4 microns. In the presence of sun-glitter the energy received by the instrument can be considered as the sum

$$E_1 = E_R + E_B + E_A + E_S$$

$$= E_o RT^2 + E_{bo} T + E_o S(1 - T) + E_S \quad . \tag{45}$$

In a region adjacent to, but clear of sun-glitter, we have

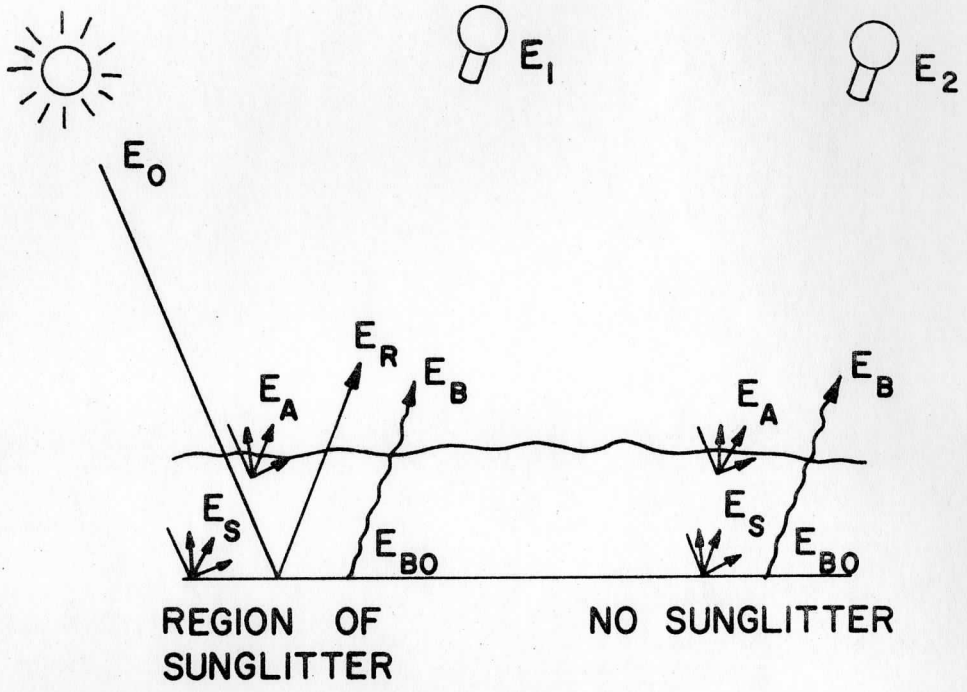

Fig. 8. Identification of the sources of radiation seen by a satellite in the spectral region of 4 microns.

$$E_2 = E_B + E_A + E_S$$
$$= E_{Bo}T + E_oS(1 - T) + E_S \qquad (46)$$

From these relations one may derive values of R and T. There are at least four ways to do this, each involving a different set of assumptions.

If T is assumed to very nearly equal 1 at 4μ, then

$$E_2 = E_{Bo} + E_S \quad . \qquad (47)$$

and

$$R = \frac{E_1 - E_2}{E_o} \quad . \qquad (48)$$

To obtain the atmospheric turbidity in the region 4000 Å to 2μ, it is now necessary to apply the proper functional relationship to the reflection coefficient measured in the 4μ window. This dependence of the reflection coefficient on wavelength between 4000 Å and 4μ must be obtained in a separate experiment from aircraft[23, 24]. For success, the experiment obviously depends on the uniformity of this functional relation over large areas of the earth's water surface, or at least the constancy in time for the same area.

An alternative method of obtaining R involves the assumption that the surface temperature and the emissivity of the earth are known so that E_{Bo} may be calculated from the Planck function. The temperature of large bodies of water and well-known ocean currents are stable and predictable over long periods. In any event, the infrared Nimbus experiments have demonstrated that it is possible to obtain accurate surface temperature measurements without the necessity for surface-based experiments [25]. Then Equation (45) gives:

$$R = \frac{E_1 - E_2}{E_o T^2} \qquad (49)$$

where from Equation (46):

$$T = \frac{E_2 - E_oS - E_S}{E_{Bo} - E_oS} \quad . \qquad (50)$$

For many sea conditions E_S can probably be neglected at 4μ. An indication of this is provided in the photographs from the Gemini missions. By knowing the geographical location of the 4μ observation, which provides the surface temperature, and the aperture of the observing instrument, one then comes to a knowledge of the atmospheric turbidity in this spectral region. Measurements in the other spectral regions are obtained as before.

The third method of obtaining R involves a separate surface-based measurement of T to calibrate the instrument. In this method an instrument previously compared with the satellite instrument for its response in the 4μ spectral region observes the sun from a suitably located surface station, off one of the western Hawaiian islands, for example. A measurement of the surface temperature and emissivity at this same location then allows direct determination of R from a simultaneous satellite measurement since all the quantities are known in the solution of the satellite measurement equations for R:

$$R = \frac{E_1 - E_2}{E_o T^2} \quad . \tag{51}$$

Furthermore, since all other quantities are known in Equation (50), E_S is measured directly

$$E_S = E_2 - E_{Bo} T - E_o S(1 - T) \quad . \tag{52}$$

The fourth alternative involves use of the 12μ window to measure the earth's black-body radiation on the assumption that T and E_S are smaller quantities at 12μ than at 4μ. The rest of the analysis proceeds as before.

These four methods of analysis could be used in judicious mixture to obtain maximum precision in the measurement of atmospheric turbidity as a function of wavelength.

It is also necessary to correct for the absorption of minor atmospheric constituents in several spectral regions to obtain the aerosol contribution. NO_2 absorbs in the visible, for example, and O_3 also has weak absorption bands between 4500 Å and 7400 Å as well as its better-known 9.6μ band.

Atomic sodium and lithium resonance lines at 5896 Å and 6708 Å must also be considered.

Beyond 4μ, since the sun's energy is exceeded by the earth's radiation, measurements of atmospheric turbidity are made directly using the earth as a source. Here the complexities of measuring the reflectivity are not present, and turbidity is obtained merely by comparison of the recorded intensity with that which should be obtained from a black body without attenuation by a turbid atmosphere. One problem in this area will be to establish the appropriate black-body curve for the earth in the long wavelength region. Recent work indicates that the earth departs from a good Planckian radiator somewhat, and it may be more advantageous to use an empirically obtained radiation curve.

The radiative transport problem, with its complexities, must be solved in an appropriate approximation to make the present measurements meaningful, but recent work in this area by Sekera [26] and by Dave [27] are applicable and will allow polarization measurements to be interpreted in terms of optical depth.

There are really two conceptually different experiments considered here: the atmospheric turbidity as a function of wavelength and the rate of change of this quantity. For the measurement of the quantity itself, the complex problem of instrument calibration enters the picture, and discussions of both accuracy and precision of the measurements are appropriate. For the other experiment on the rate of change of atmospheric turbidity, just precision enters, because this measurement depends only on the long-term stability of the instrumentation, and calibration is likely to be more simple.

IV. TURBIDITY FROM ATS MEASUREMENTS

A pilot program in detecting local atmospheric pollution over metropolitan areas was begun by analyzing radiance data from the Applications Technology Satellite III (ATSC) system. Computer programs and other data reduction procedures were set up in order to correlate statistically the radiance values throughout a day over three nearby regions of different brightness levels. These regions were water (a 60 × 60 km area in the Pacific Ocean off Baja, Mexico), city (the metropolitan Los Angeles area), and desert (a relatively flat region in the Altar Desert). 23 April 1968, a cloud-free day over the three regions under study, was chosen as the day for analysis. It was found that the radiance over metropolitan Los Angeles decreased throughout the day, whereas the radiance relative to the referenced areas increased, implying that the turbidity over Los Angeles also increased. Correlation with visibility data for that day, however, is not good, possibly because 23 April was not a particularly smoggy day. An effort is being made, therefore, to locate data for a day which may illustrate the method better.

Introduction

No attempt has been made to date to correlate satellite radiance data with local conditions of turbidity. Since there has been no satellite launched which has as its primary objective the detection of local air pollution, or for that matter even global pollution, it seems therefore reasonable to attempt to determine if it is indeed possible to observe local atmospheric turbidity from data taken by a currently operating satellite which has optical detectors aboard, even though these detectors were not primarily designed for haze observations. The reason behind the choice of studying the turbidity build-up and dissipation over a large metropolitan area is that the results may be correlated with the

various ground atmospheric measurements that are usually made on a continuous basis within cities. Almost invariably the daily change in atmospheric haze over cities exceeds the change over woods, deserts, and water, so that these areas constitute likely reference areas. In an initial attempt at the satellite radiance variation problem over local terrain, then, it was felt that it would be of interest to compare the results of three areas: city, water and desert. The albedo over the ocean is quite small (as long as observation takes place away from sun-glitter areas), whereas the albedo over the desert is quite high, and that of the city is in between these two. These expectations are borne out in the results. The major problem in the data analysis was found to be in navigation. Navigation in this sense refers to alignment of the line and element matrix of the satellite data with the geographic points of latitude and longitude. This will be discussed in detail below. The data initially indicates that haze growth over Los Angeles on 23 April 1968 was detected, based on an increase in the relative reflected radiance as received by the satellite after sun-angle effects have been accounted for. This tentative conclusion must be heavily qualified, however, until an analysis of several other days can be made.

The Satellite and Camera System

The Applications Technology Satellite III (ATS-III) is the third of a series of ATS scientific satellites built for the National Aeronautics and Space Administration, Goddard Space Flight Center. The basic ATS-III spacecraft is a cylinder 54 in. long and 57.6 in. in diameter with its spin stabilized at a nominal 100 rpm and its spin axis aligned with that of the earth. The spinning spacecraft acts as a free gyro; however, two independent 5-lb. thrust control jet subsystems may be used for adjustments in oribital inclination and/or eccentricity, thereby maintaining the satellite spin axis in the desired orientation in inertial space. A network of six ground stations supports the ATS operation. Two stations assume responsibility for tracking the spacecraft during its normal scientific lifetime, controlling the spacecraft, conducting experiments and recording and processing spacecraft housekeeping data. The

two controlling ground stations are located at Rosman, North Carolina and Mojave, California. The Rosman ground station assumes primary responsibility for the acquisition of the Multicolor Spin Scan Cloud Camera (MSSCC). It acquires the data from the spacecraft by means of digital and analog tape records. The data from 23 April 1968 is on raw digital tapes stored in the computer center at the Space Science and Engineering Center. The view of the earth from the ATS-III satellite at earch synchronous height is similar in many respects to that of the moon viewed from the earth. The satellite was located on 23April 1968 over the equator at 60° west longitude.

The Multicolor Spin Scan Cloud Camera consists of a high resolution telescope, three photomultiplier light detectors, and a precision latitude step mechanism. The latitude step motion, combined with the spinning motion of the ATS satellite, permits scanning a complete earth disc. The area is swept out by 2400 horizontal (west to east) scan lines. The ground resolution is 2 nautical miles at the subsatellite point. The optical system consists of a primary 5-in. elliptical mirror and a secondary 1.82-in. spherical mirror, which has a focal length of 15 in. Light is directed onto an image plane where three 0.0015-in. diameter field-defining apertures are placed 0.010 in. apart. The primary mirror, the secondary mirror and the aperture plate are made of fused silica to provide optimum dimensional stability. Each aperture defines a color signal and the physical displacement of the apertures in the optical system results in a short time delay between the color signals from the same point. The radiant energy collected by the moving telescope is transmitted by fiber optics to stationary photomultiplier tubes. The MSSCC video circuitry consists of identical amplifier channels for each of the three colors, red, blue and green.

The spectral response as a function of wavelength is shown in Fig. 9. A single sun-pulse amplifier supplies sun-synchronizing pulses to the red and green video channels. The data analysis in this paper concerns only the green channel. Three analog time division multiplexed color signals are normally generated with each revolution of the satellite. The signals are demultiplexed on the ground and sent through separate analog to digital converters. The

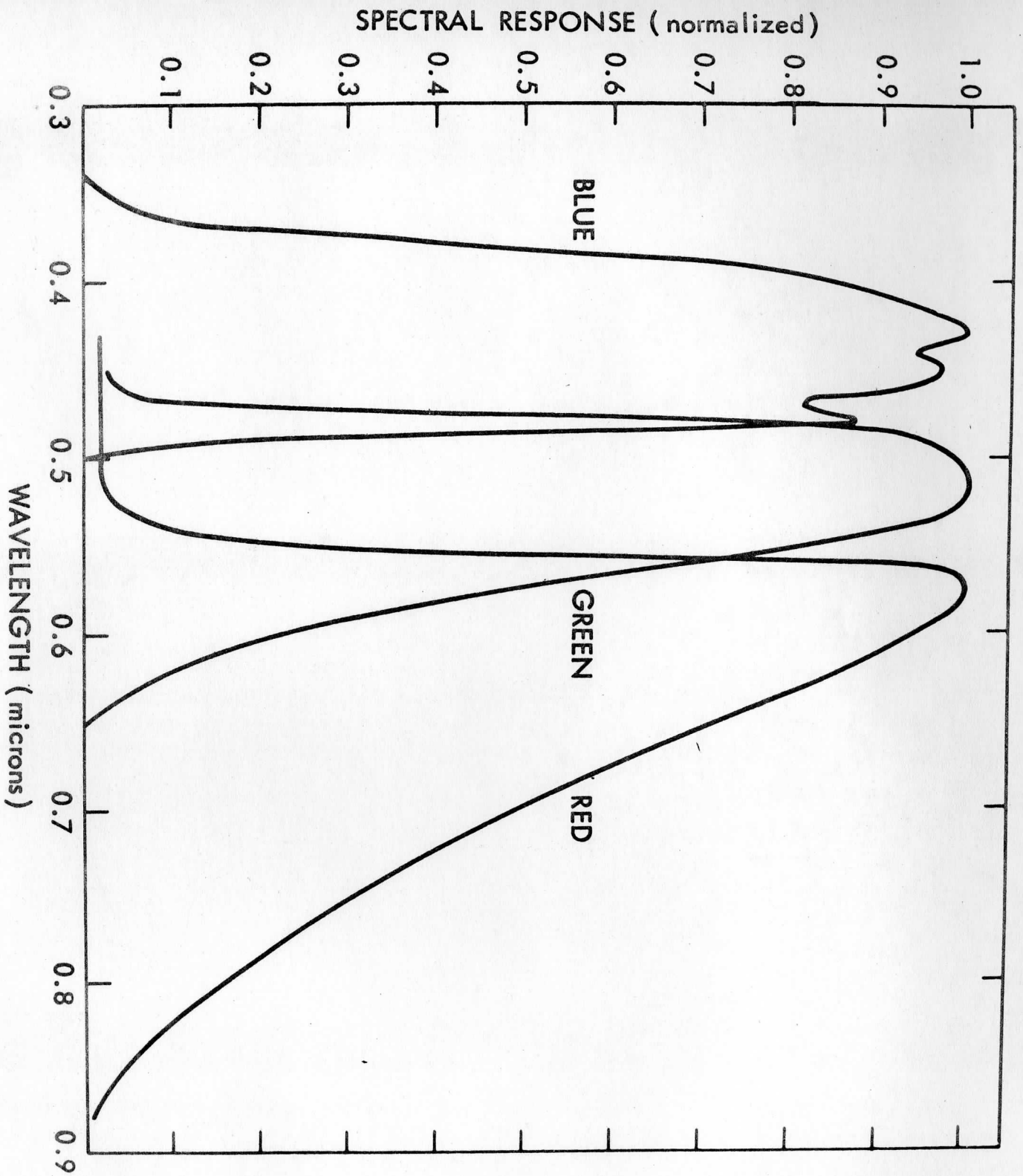

Fig. 9. Spectral Response vs. Wavelength.

converted signals are then stored in a buffer which is unloaded during the back scan of the camera in sequential order to the on-line digital tape recorder. The ATS-III MSSCC picture of the half-scan earth disc for 23 April 1968 is shown in Fig. 10. The cloud-free California-Baja area can be seen in the upper left-hand area.

Data Analysis and the Navigation Problem

Two multi-usage programs have been written and debugged for use in the alignment of ATS pictures and in the averaging and sampling process of data reduction of radiance values. These two programs, written in Fortran V, may be run on the University of Wisconsin Computer Center's Univac 1108 system or on the Space Science and Engineering Center's Raytheon 440 system.

The first program, named ATSTIX, is designed to reduce ATS digital data tapes so that only one data card characterizes each area under consideration. The analysis of the raw data consists of performing various kinds of averaging statistics and grid plots within previous chosen brightness ranges. One important example of this multi-purpose program is shown in Fig. 11. This is a frequency distribution plot of brightness levels over a small portion (Southern California-Baja area) of the ATS satellite radiance photo on 23 April 1968. Computer graphing of the frequency distribution in this manner allows us to determine more accurately the enhancement parameters to use in expanding the brightness levels so that water-land and/or woods-city areas may be made distinguishable. This is directly related to the navigation problem.

The second program, named ATSPST, is designed to read ATS digital data tapes such that the brightness levels may be mapped into letters of corresponding optical density, and then to print out these letters in a grid matrix on the 80-column printer of the Raytheon 880. This program is the primary means of navigating each tape to achieve a precise alignment of local latitudinal and longitudinal coordinates with the ATSC line and element grid. Averaging over certain prechosen areas for a series of ATSC digital data tapes is shown in

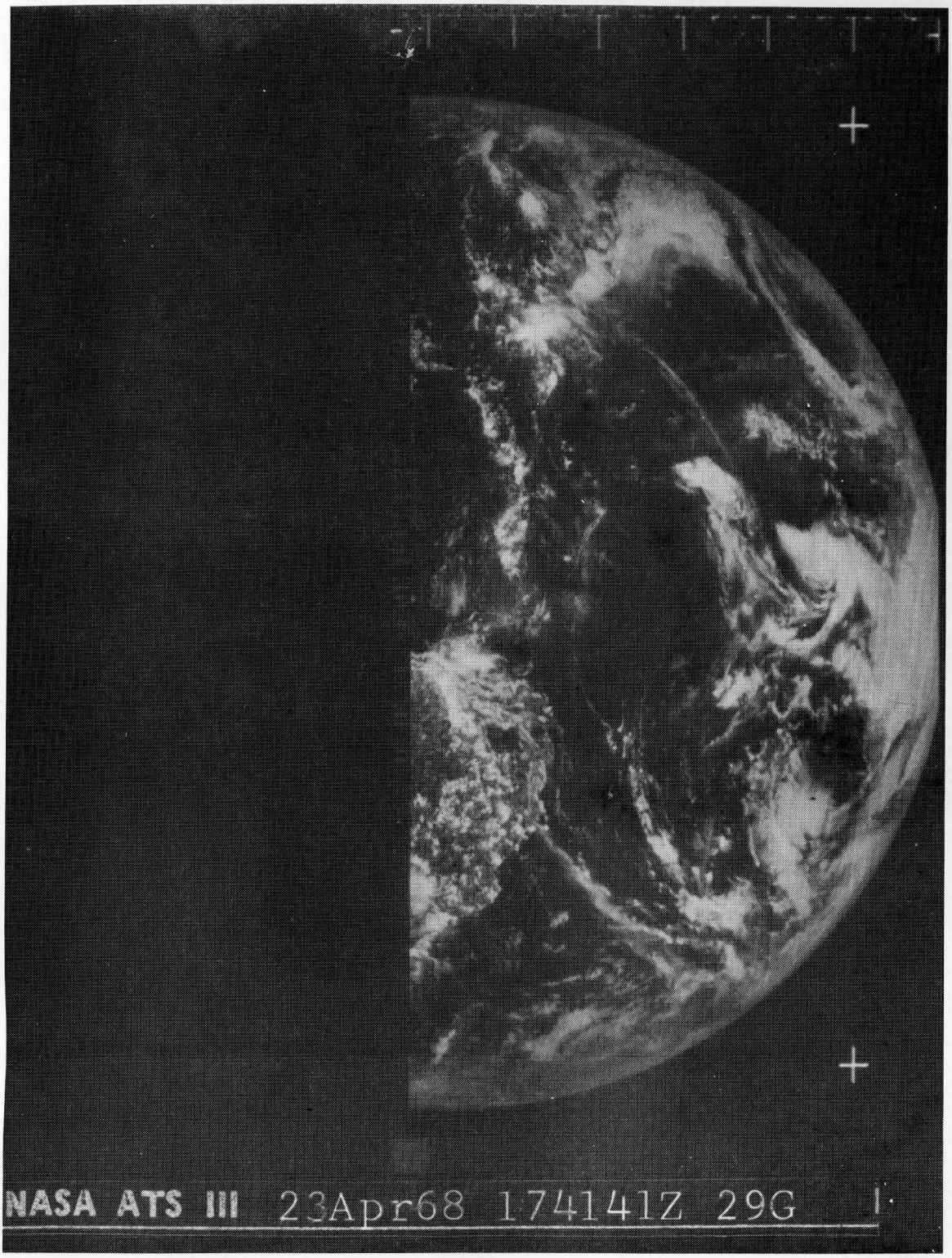

Fig. 10. An Applications Technology Satellite III (ATSC) half-disc picture of the earth taken on 23 April 1968. Note the cloud-free area of the Baja Peninsula and southern California in the upper left-hand region. This is using the Green channel of the Multicolor Spin-Scan Cloud Camera.

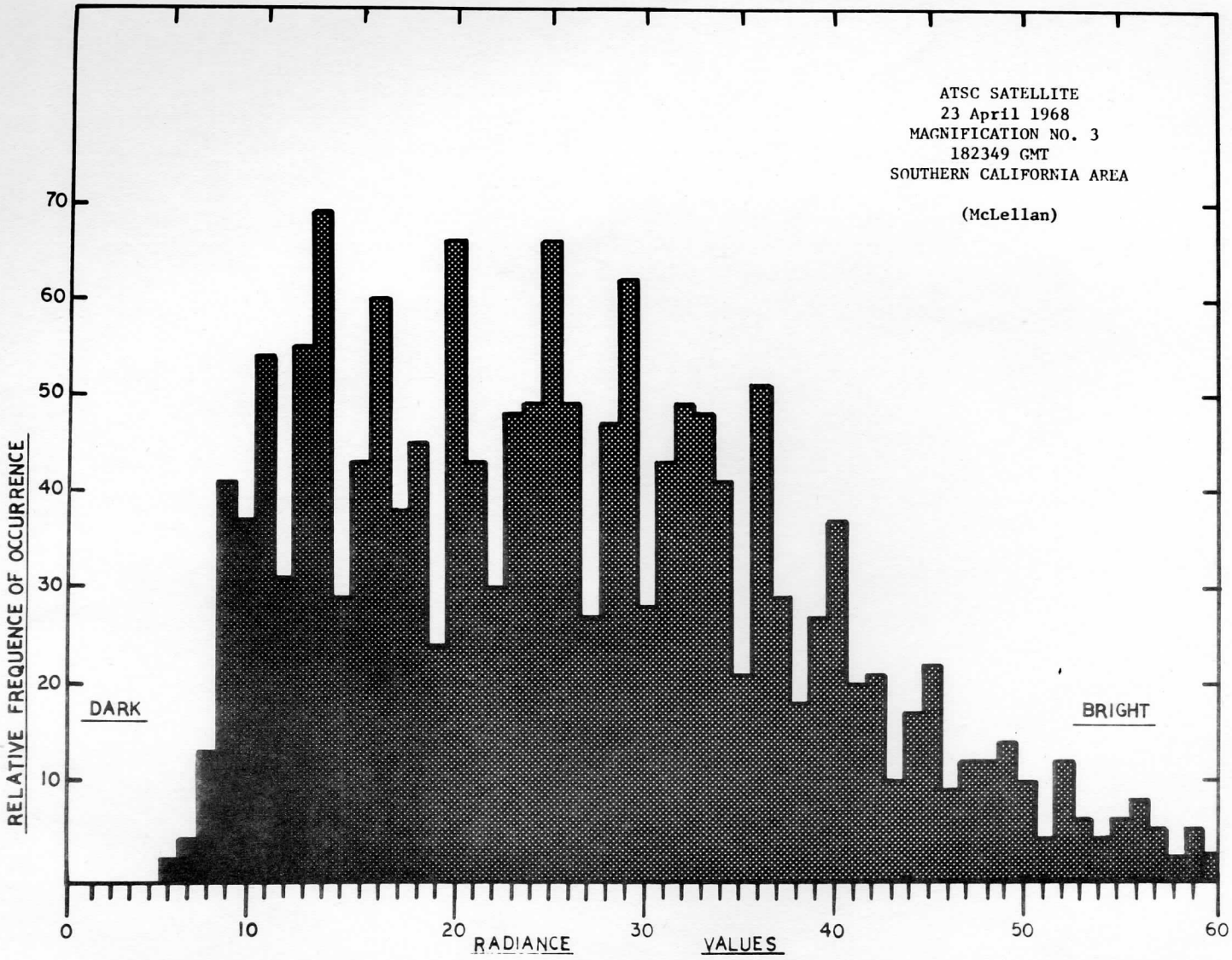

Fig. 11. A frequency distribution plot of brightness levels over the Southern California Baja area. These plots serve to locate the cutoff between sea and land for purposes of enhancement.

Fig. 12, where each point on the graph represents an average radiance value over Los Angeles, the Altar Desert, or an area of the Pacific Ocean near Baja for each satellite tape throughout the day of 23 April 1968.

In conjunction with the ATSPST program, a program has been developed whereby navigation is done by means of viewing a computer-generated photo-facsimile photograph of a desired area at a predetermined magnification so that proper enhancement parameters may be thus chosen and landmarks may be thus found. Figure 13 shows a computer-generated photo-facsimile of the Southern California area, where the islands, Santa Catalina, Santa Cruz and San Clemente off the coast near Los Angeles can clearly be seen and identified for navigational purposes. In this manner it is possible to align data from various ATSC tapes to within two lines and two elements.

In order to make full use of ATS tapes it is very important that precise navigation be done by computer. However, so far this has not been feasible. In cloud movement studies, which is the primary purpose of the ATS series of satellites, precise navigation on the order of two lines and two elements is not necessary. But in the study of radiance measurements from localized areas on the order of 10-30 km, it does indeed become very important. Initial steps in computer navigation have been made, but so far it has been unsuccessful in precision navigation.

A preliminary attempt [28] to align two ATS pictures relative to each other in a computer, rather than align each of them relative to the earth, by means of computer searching the limb of the earth has been somewhat successful in cloud wind velocity studies. This is a two-step process, the first of which matches two earth edge points (one from each of two tapes) and is done simply by line and sample transformation, not by rotation or magnification. The earth edge for each line is defined as the first point where three consecutive samples have a radiance level of five or greater.

The second step involves locating the minimum sum of absolute differences between the two tapes of each of the sample's radiance values in two matrices,

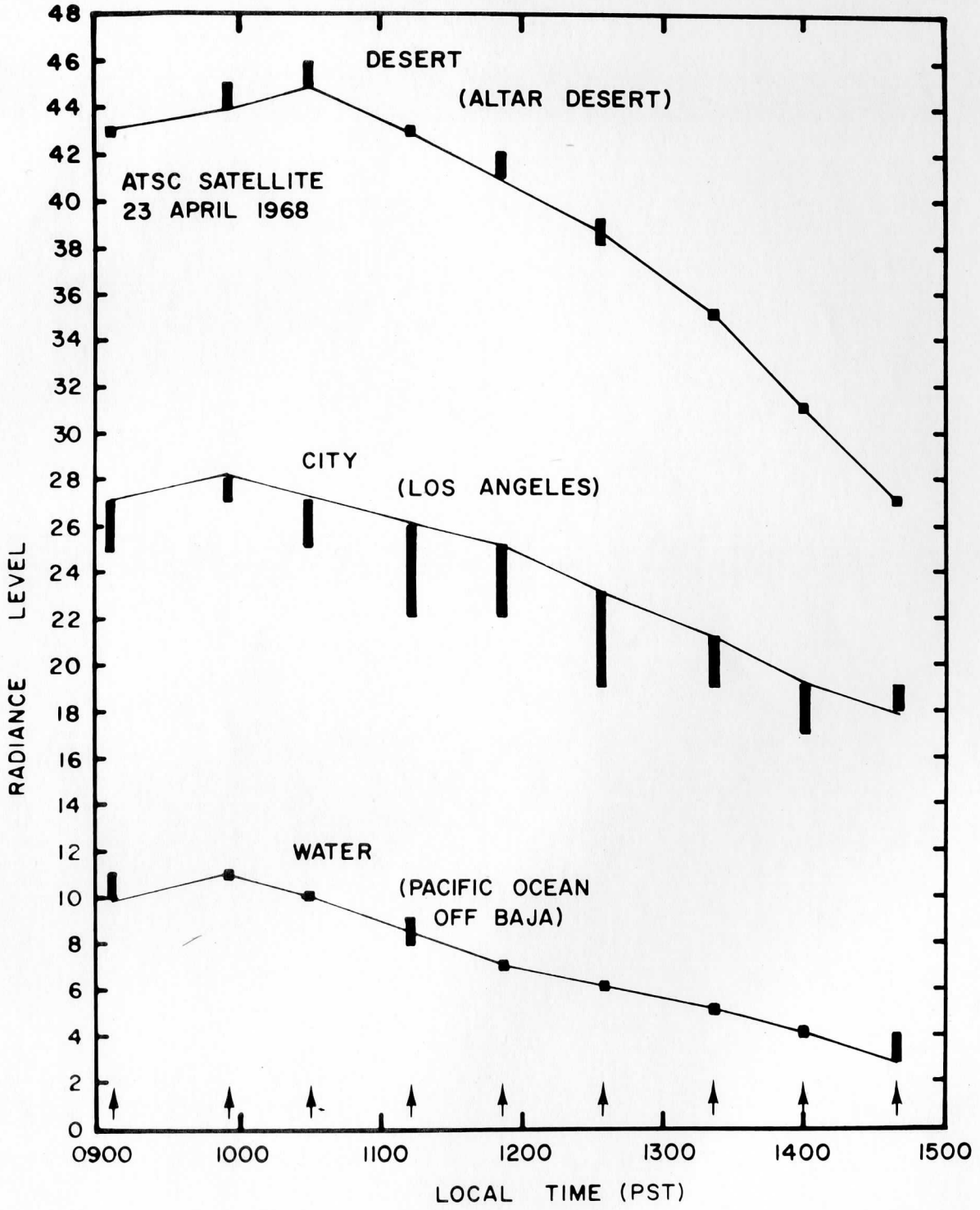

Fig. 12. Raw Average Radiance levels from the green channel of the Multicolor Spin-Scan Cloud Camera throughout the day of 23 April 1968. In each of the three regions for each picture, the areas were reduced in size until a convergence limit was reached for the averaged brightness. These limits are connected by straight lines.

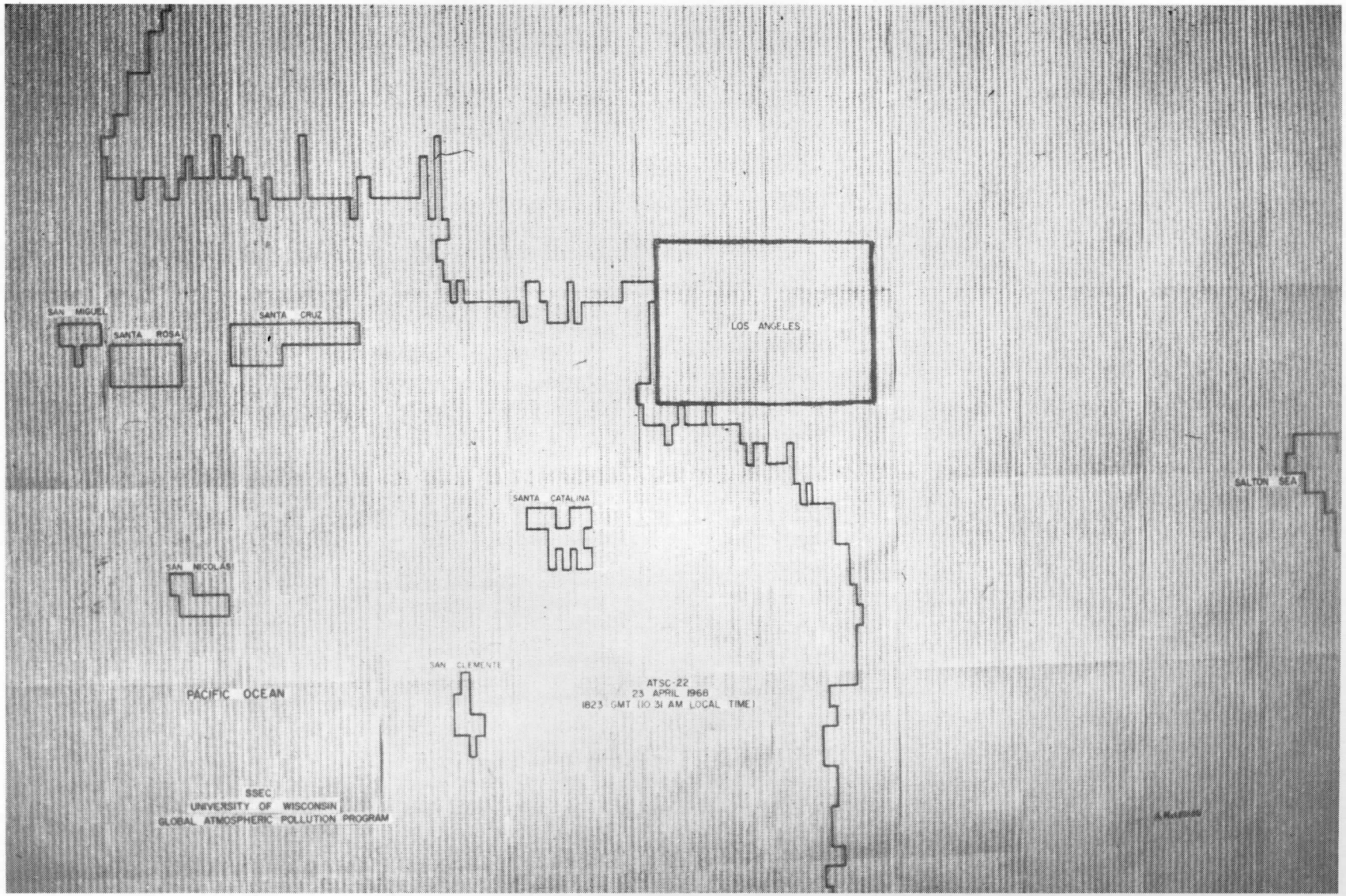

Fig. 13. A data display of the actual brightness values over the southern California region is used for navigation purposes. Familiar landmarks are clearly visible. From this display one can see the resolution at this latitude of the Multicolor Spin-Scan Cloud Camera.

which are centered on and follow the earth edge. The first step is used as an initial guess for the second step. However, the precision achieved in this work is not sufficient for the alignment required for local air pollution detection.

Results

Throughout the day of 23 April 1968, the reflected earth radiance as seen from ATS-III satellite from the Altar Desert (top curve), the Los Angeles metropolitan area (middle curve) and an area in the Pacific Ocean near Baja (bottom curve) is shown in Fig. 12. Experimental points represent the mean of the two extreme values shown as horizontal dashes, and the solid lines are drawn through the values to which the data appeared to converge and successively smaller sample areas were taken around a common center. The obvious decrease in radiance values throughout the day for all curves is probably due largely to the changing sun angle. In the early morning the satellite-Los Angeles-sun angle is at a minimum, and in the late afternoon this angle reaches its maximum value.

Since the albedo of the Altar Desert is high, the change in radiance from this area throughout the day represents predominantly the change in surface brightness with sun angle. But because of the low albedo of the ocean surface, the change in radiance from the area offshore represents a greater proportion of the effects attributable to atmospheric scattering.

It is instructive to calculate the percentage change in radiance values of the bright area (the desert) and the dark area (the water), and then from these results interpolate the values for the Los Angeles area (see Table 1). In this crude way one may attempt to compensate for the sun angle variance, assuming that the intensity of scattered light from haze is much less over the water and the desert than it is over the city.

Correlation with ground visibility data is not good. This first, rather hasty attempt was performed for a day on which there was no serious smog in the Los Angeles basin, however. If data are available for a smoggy day, it is planned

Table 1. Interpolated Radiance Values over Los Angeles, 23 April 1968

Local Time (PST)	Bright Area (Desert) % change from median value	Dark Area (Water) % change from median value	Los Angeles interpolated radiance values	Visibility* (miles)	Visibility+ (miles)
8:00 AM				10.0	10.0
9:09 AM	16.3	30.0	20.8		
9:51 AM	18.2	36.3	20.4		
10:00 AM				15.0	12.0
10:31 AM	20.0	30.0	20.3		
11:00 AM				20.0	20.0
11:13 AM	16.3	12.5	22.3		
11:54 AM	12.2	0.0	23.5		
12:00 noon				20.0	20.0
12:37 PM	-1.8	-16.7	23.4		
1:00 PM				20.0	25.0
1:18 PM	-2.9	-40.0	25.5		
2:00 PM	-16.1	-75.0	27.7	25.0	20.0
2:42 PM	-33.3	-133.0	33.0		
3:00 PM				20.0	15.0

*Weather Bureau visibility data at Los Angeles International Airport.

+Los Angeles County Air Pollution Control District visibility data for downtown Los Angeles.

to conduct the same analysis in an attempt to obtain a quantitative measurement related to an optical index of pollution.

V. TECHNIQUES FOR REMOTE SENSING OF GASEOUS AIR POLLUTANTS

In the last few years a number of new techniques have been developed for remote sensing of both gaseous and particulate pollutants in the atmosphere. Most of these techniques apply to short-range (of the order of a few km at the most) remote sensing and are not in their present stage of development suitable for adaptation for satellite surveillance of global air pollution. Ludwig, Bartle and Griggs [29] have carried out a detailed study of several remote sensing techniques in their comprehensive report "Study of Air Pollutant Detection by Remote Sensors," (1968). In this report the several instruments considered in detail include 1) the ordinary dispersion type spectrometers, 2) filter wedge spectrometers, 3) multiple detector spectrometers, 4) scanning spectrometers, 5) interferometer spectrometer (Michelson type), 6) correlation spectrometer, 7) matched filter spectrometer with multiple entrance slits, 8) selective chopper radiometer, and 9) the cross correlating spectrometer.

The correlation spectrometer first developed by Barriger Research Ltd. [30] has been used for remote sensing of gaseous pollutants, particularly SO_2 in metropolitan areas. It has been proposed that the method can be applied to study the concentration of carbon monoxide via the 2.3μ overtone band of the 4.7μ fundamental, using the solar radiation backscattered by the atmospheric constituents as the source. Improvements in the Barringer technique have been attempted by Williams and Kolitz [31] and it has been claimed that parts per billion concentration of some minor constituents can be measured. Ludwig, et al. have also attempted improvements on the basic Barringer technique for the IR region with a matched filter spectrometer and multiple entrance slits and with selective chopper radiometers with multiple cells. These methods appear to be suitable for satellite applications.

V. TECHNIQUES FOR REMOTE SENSING OF GASEOUS AIR POLLUTANTS

In the last few years a number of new techniques have been developed for remote sensing of both gaseous and particulate pollutants in the atmosphere. Most of these techniques apply to short-range (of the order of a few km at the most) remote sensing and are not in their present stage of development suitable for adaptation for satellite surveillance of global air pollution. Ludwig, Bartle and Griggs [29] have carried out a detailed study of several remote sensing techniques in their comprehensive report "Study of Air Pollutant Detection by Remote Sensors," (1968). In this report the several instruments considered in detail include 1) the ordinary dispersion type spectrometers, 2) filter wedge spectrometers, 3) multiple detector spectrometers, 4) scanning spectrometers, 5) interferometer spectrometer (Michelson type), 6) correlation spectrometer, 7) matched filter spectrometer with multiple entrance slits, 8) selective chopper radiometer, and 9) the cross correlating spectrometer.

The correlation spectrometer first developed by Barriger Research Ltd. [30] has been used for remote sensing of gaseous pollutants, particularly SO_2 in metropolitan areas. It has been proposed that the method can be applied to study the concentration of carbon monoxide via the 2.3μ overtone band of the 4.7μ fundamental, using the solar radiation backscattered by the atmospheric constituents as the source. Improvements in the Barringer technique have been attempted by Williams and Kolitz [31] and it has been claimed that parts per billion concentration of some minor constituents can be measured. Ludwig, et al. have also attempted improvements on the basic Barringer technique for the IR region with a matched filter spectrometer and multiple entrance slits and with selective chopper radiometers with multiple cells. These methods appear to be suitable for satellite applications.

The interferometer spectrometer of the Michelson type has been applied with commendable success for temperature sounding of the atmosphere using the measurements in the 15μ band of carbon dioxide. Normally the instrument covers the entire infrared spectrum between 5 and 20 microns. The fundamental absorption band of carbon monoxide lies in the vicinity of 4.7 microns. If the spectral range of the interferometer spectrometer can be extended to cover this region, then the high resolution spectra obtained with such an instrument can be used for constituent inversion. This region is not of particular interest for temperature inversion studies. However, a simple extension of the spectral region should not present major difficulties and will not affect adversely the temperature sounding experiments. The main advantage of the interferometer spectrometer is the high resolution obtainable leading to high specificity in the determination of concentration of particular constituents. The complexity of the instrument and the involved procedure with Fourier Transforms to recover the spectra should be weighed against this important advantage. In fact, one of the three main objectives [32] of the Infrared Spectroscopy Experiment for Mariner Mars 1971 [33] is measurement of minor atmospheric constituents using a Michelson type interferometer spectrometer operating in the spectral range 200 to 1600 cm^{-1}. If the minor constituents of the martian atmosphere can be probed from an orbiting spacecraft, it is reasonable to believe that it should be possible to probe the earth's atmosphere as well.

Almost all the remote sensing methods proposed for monitoring global air pollution involve measurement of the radiation that the space-borne instrument will receive looking down towards the earth either at a constant angle or in a scanning mode. Because of the very low concentration of the pollutant gases, the instrument sensitivity should be very high and the interference from other constituents should be avoided as much as possible. These requirements impose severe constraints on the instrumentation. However, if measurements could be made through the limb of the earth using the sun as the source of radiation, the optical path length can be considerably increased and signal-to-noise ratio improved. There are problems both theoretical and experimental

connected with measurements through the atmospheric limb. Since the temperature, pressure and concentration of the constituents vary along the path of observation, the interpretation of the observed transmission of selected radiation intervals in terms of the total concentration of the absorbing constituents is somewhat complicated. Detailed methods for computing transmission of infrared radiation through atmospheric slant paths have been developed and reported particularly by Drayson [34], Anding [35] and others. Even though the formulas are well developed from theoretical considerations, the computation of transmissions in the case of some pollutant molecules is difficult due to insufficient data on the molecular parameters such as line strength, line shape, half widths, etc.

The width and shape of an absorption line is influenced by collisional or Lorentz broadening and by Doppler broadening arising from the motion of the molecules. The relative importance of Lorentz and Doppler broadening depends on the region of the atmosphere under consideration. In the optically thick layers of the lower atmosphere where collisions are frequent, the broadening is predominantly Lorentz in character. At very high levels, on the other hand, Doppler broadening is important while at intermediate heights a combination of both Lorentz and Doppler effects is present.

At a particular frequency interval $\Delta\nu$ the transmissivity, τ, is given by the relation

$$\tau(x, \nu) = \frac{1}{\Delta\nu} \int_{\Delta\nu} \{\exp[- \int_0^x k(x, \nu)\rho(x)dx]\}d\nu \tag{53}$$

where $\rho(x)$ is the density of the absorbing gas, x the distance along the path, and $k(x, \nu)$ the absorption coefficient.

The form of $k(x, \nu)$ from Lorentz theory is

$$k(x, \nu) = \frac{S}{\pi} \frac{\alpha_L}{(\nu - \nu_0)^2 + \alpha_L^2} \tag{54}$$

where ν_0 is the frequency of the line center, S is the line strength, and α_L

is the Lorentz half-width.

For a Doppler broadened line

$$k(x, \nu) = k_0 e^{-y^2} \tag{55}$$

where

$$k_0 = \frac{S}{\alpha_D} \left(\frac{\ell n\, 2}{\pi}\right)^{1/2}; \qquad y = \frac{\nu - \nu_0}{\alpha_D} (\ell n\, 2)^{1/2} \tag{56}$$

and α_D, the Doppler half-width is given by

$$\alpha_D = 3.58 \times 10^{-7} \left(\frac{T}{M}\right)^{1/2} \nu_0 \tag{57}$$

M = molecular weight.

For a mixed Lorentz Doppler line, the Voigt profile describes the line shape:

$$k(x, \nu) = \frac{k_0 u}{\pi} \int_{-\infty}^{\infty} \frac{e^{-t^2}}{u^2 + (y - t)^2}\, dt \tag{58}$$

where

$$u = \frac{\alpha_L}{\alpha_D} (\ell n\, 2)^{1/2} . \tag{59}$$

If the spectral interval contains many lines, then we can compute the total transmission by making line-by-line computations or by making simplifying assumptions comprising the various band models and combine these with integration over the observed path. This computation can become quite time consuming even for fast digital computers.

Raman spectrometric techniques using a combination of high-powered lasers and specialized optics and electronics have been recently suggested [36] for remote sensing (short range) of pollutants. The Raman technique more or less follows as a logical extension of the lidar technique applied for remote sensing of aerosol layers in the atmosphere.

There are a number of advantages in favor of the Raman technique. In particular, it has a high degree of specificity and the Raman-shifted frequencies bear an accurate signature of specific molecules. It is insensitive to

fluctuations in temperature and pressure in the measured volume.

The method may be well suited for analyzing mixtures whose components can be assumed and whose concentrations have to be determined and the installation and operation of high-power laser systems is not a major problem.

For satellite applications, the Raman technique may be ruled out for the immediate future because of the small value of Raman scattering cross-sections, and because of problems involved in the installation and operation of high-power lasers from spacecraft.

Another system which has potentialities for space applications is the Hadamard Transform Spectrometer [37] which can combine the multiplex properties of the Michelson interferometer and yet be able to reject all spectral information not of direct interest in the analysis. This system is in the early stages of development and perfection, but has already been applied successfully for automobile exhaust analysis.

VI. MEASUREMENT OF CO FROM SMS SATELLITE

This section offers a description of a relatively simple system that will provide continuous surveillance of local and global horizontal movement of carbon monoxide pollution in the earth's atmosphere. It is also proposed that this sytem can be conveniently integrated within the Geosynchronous Meteorological Satellites' (SMS) infrared spin scan radiometer, for which funds have already been allocated by the National Aeronautics and Space Administration.

Estimates are made of the pertinent parameters (such as CO concentrations, black-body radiation emission from the CO band, figure of merit (D^* normalized detectivity)), and descriptions of the materials necessary for adapting the system to the SMS type of spin scan camera (such as fiber optical transmissions and filter requirements).

Geosynchronous Meteorological Satellite (SMS)

The National Aeronautics and Space Administration (NASA) has approved plans for the launching of two Geosynchronous Meteorological Satellites (SMS) in 1971-1973 to carry on the work of the very successful ATS-I and ATS-III spin scan camera in monitoring weather patterns on earth [38]. This type of synchronous satellite has the advantage of obtaining quick synoptic scans as well as being able to pinpoint fast changing pollution and weather situations. An additional advantage of such a multispectral system is that the data collected from its various bandwidth detectors eliminate the difficulty of data correlation with other satellites. The SMS system to be launched first is designed as a basic monochromatic instrument following an improved spin scan camera which has higher resolution in the visible light channel and a new infrared nighttime imaging capability. This will be a modification of the earlier

Santa Barbara Research Center [39] design called VISSR (Visible and infrared Spin Scan Radiometer). An outline of this radiometer is sketched in Fig. 14. A schematic of the aft section is located in Fig. 15.

Atmospheric Concentration of Carbon Monoxide

World-wide surface concentration of carbon monoxide in remote areas has been measured over the last twenty years by a number of investigators [40-46]. It was found, on the average, that CO is fairly uniformly distributed throughout the atmosphere and that the concentration is on the order of 0.08 to 0.10 parts per million. This shows that CO is a world-wide constituent of the atmosphere of considerable concentration compared to other trace substances. However, very little is known about the production and destruction rates of CO. The concentration of atomic oxygen, the oxidation properties of ozone, bacterial activities and photochemical processes are all too uncertain to estimate global production and destruction rates based merely on laboratory experiments. To date, no measurements have been made to monitor carbon monoxide on a global scale, although one experiment is currently in the planning stage. Many speculations exist as to the overall global distribution of CO [47, 48], but all these theories are based on very little data. The presently conceived experiment offers the first step to make this fundamental determination simply and quickly.

The Carbon Monoxide Spectroscopic Band [49-52]

Carbon monoxide, a primary pollution component, has its strongest absorption-emission band at 4.6μ, which is located in an atmospheric window and therefore it is an ideal candidate for satellite measurement.

In the short wavelength wing of the CO band lies a strong band of N_2O [53]. Nitrous oxide, a stable gas, is generally believed to be somewhat uniformly distributed throughout the earth's atmosphere with a mixing ratio such that its global average concentration is on the order of 0.40 ppm [54-56]. The 6.3μ band of H_2O enters in the long wavelength wing of the CO band [53]. However,

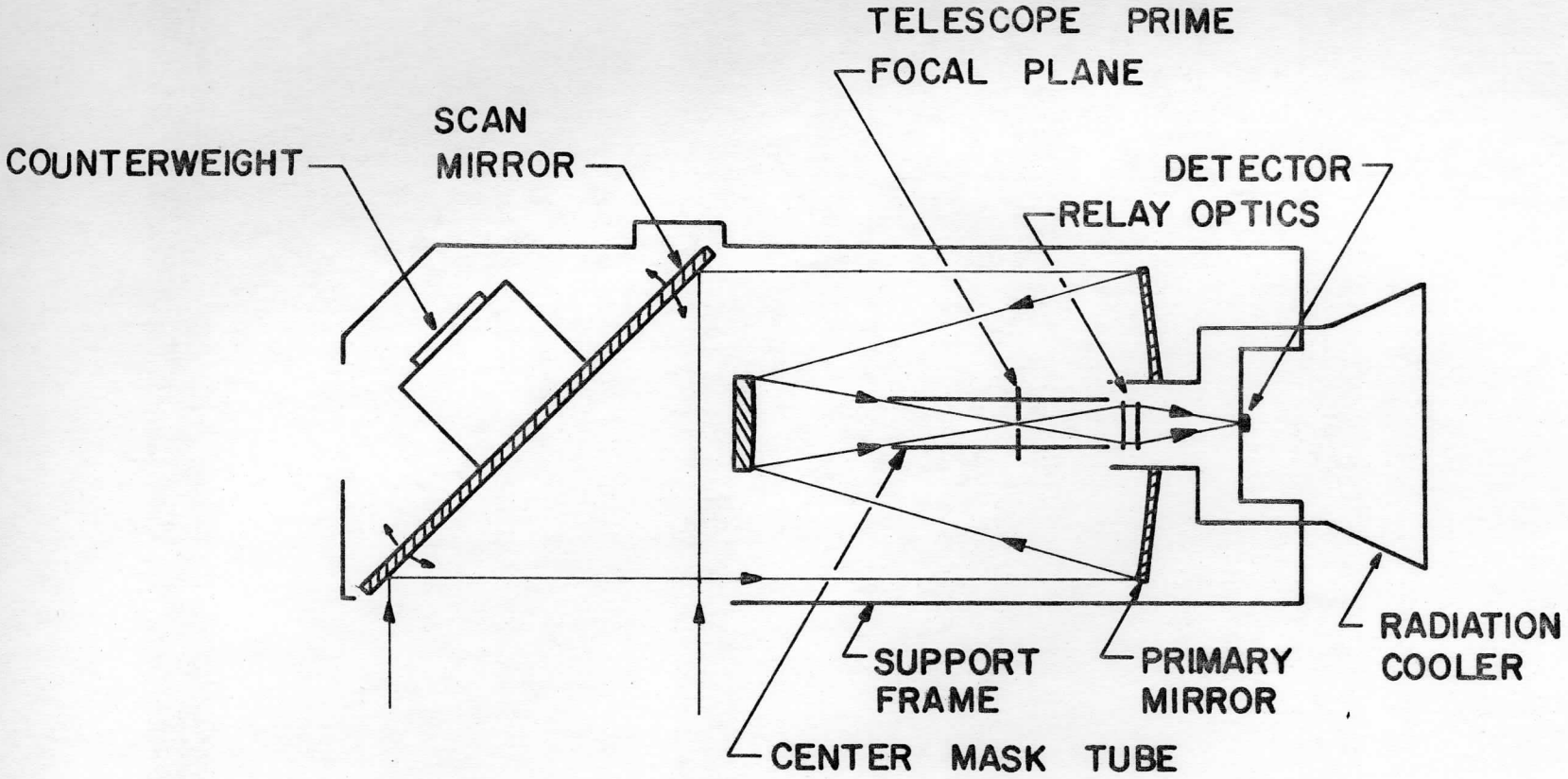

Fig. 14. Visible Infrared Spin-Scan Radiometer for a Synchronous Meteorological Spacecraft.

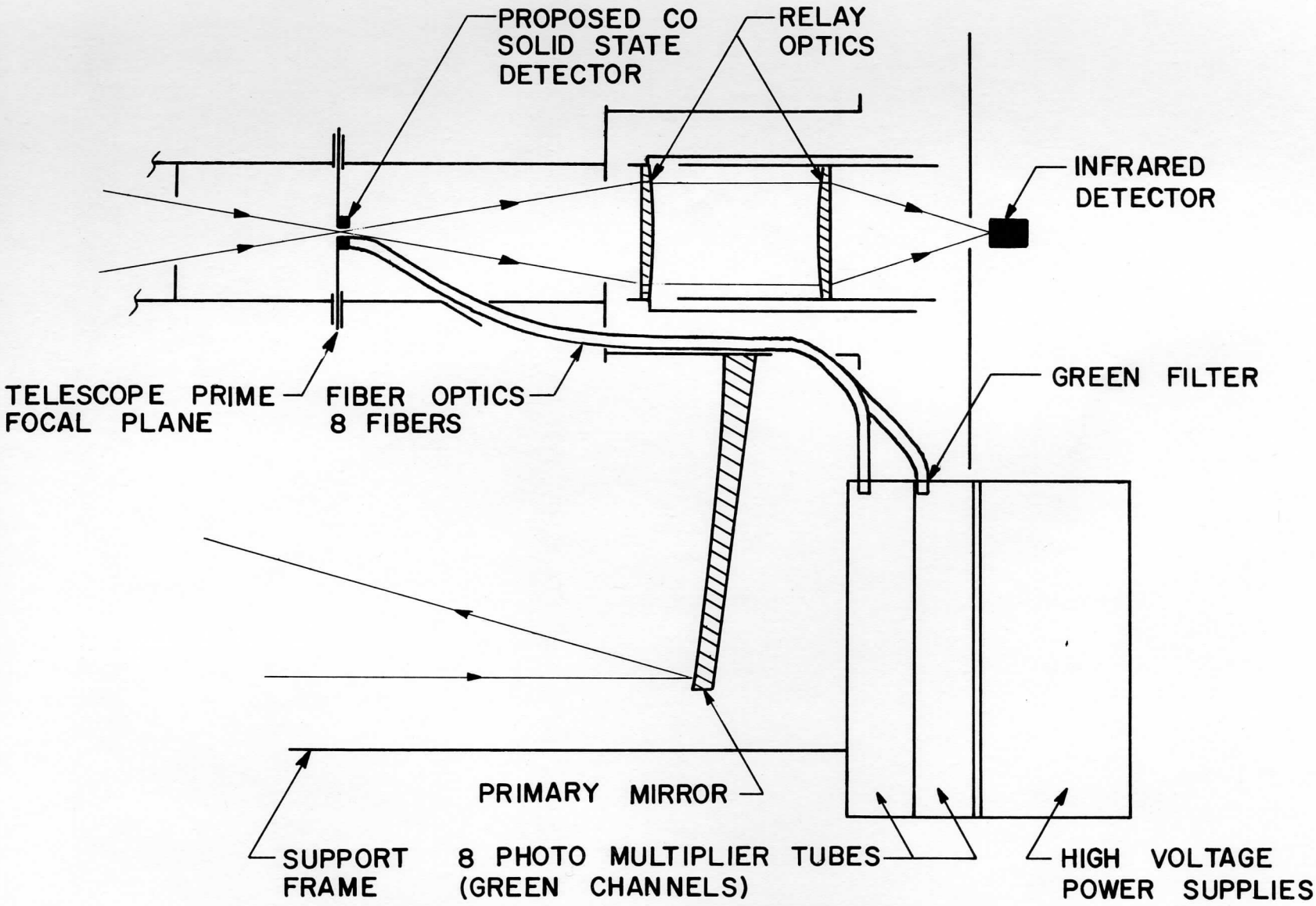

Fig. 15. Radiometer Aft Optics Detail.

with a judicious choice of detector (or filter) bandwidth, or possibly with the use of two or three detectors, one can overcome the problem of interference from these two other atmospheric constituents.

Fiber Optics

To facilitate the adaptation of a 4.6μ detector to the SMS VISIR (Visible Infrared Sounding and Imaging Radiometer) system, it will possibly be advantageous to employ fiber optics as the primary light transmission part of the instrument. This will allow ease in adapting a CO detecting apparatus to a fixed SMS system.

A. Infrared Fiber Optics

For wavelengths beyond about 2.5μ where most optical glasses attenuate rapidly, one must consider other kinds of fiber materials. Work has been done on doped germanium and calcium aluminate glasses in order to extend the infrared transmission out to about 5μ. However, transmission still further into the infrared has been achieved by using arsenic trisulfide glass [57]. Fibers having a stoichiometric As_2S_3 glass core (index of refraction n = 2.47) and a modified arsenic sulfide coating (n = 2.416) transmit out to 7μ for a fiber length of 0.5 meter. These types of fiber have been prepared at the American Optical Co.

B. Polychromatic Fiber Optics

A single-ratio polychromatic fiber optics component consists of a mixture of two types of elemental fiber. Each fiber type covers a certain spectral range, and so the macroscopic spectral transmittance of the final component is the total of the weighted spectral transmittances of the constituents. The spectral transmittances of a variable-ratio polychromatic fiber optics component will provide a wider spectral range than that available with standard fiber optic components. Thus, a fiber could be developed such that the transmittance is enhanced in the 4.7μ region and also enhanced in a nearby region, such as in an atmospheric window or in the short wavelength wing of the CO band at the N_2O band peak.

Detectors

In order to prevent an increase in the presently planned cooling load of the S. M. S. passive radiative cooler, it is preferable not to add another detector to the cold finger of the S. M. S. This limits the choice of ultra-sensitive spectral detectivities as well as the spectral response. However, lead selenide detectors, from the Santa Barbara Research Center [58] operating at ambient temperature (295° K Nominal) have a satisfactory spectral response for carbon monoxide detection (see Fig. 16). The time constant for this detector is on the order of 2μ sec., which is less than the maximum response time of 4.2μ sec set by the spin cycle of the SMS infrared imaging radiometer.

Radiation from Earth

It is necessary to determine the amount of radiation reaching the satellite near the 4.7μ band in order to make a decision as to the necessity of employing a cooled detector for the CO absorption. The calculations below are very rough and are used to get a feel for the magnitudes involved.

The energy at wavelength λ received by a satellite through the atmosphere can be expressed approximately by the formula [29]

$$E_\lambda(T_0) = \epsilon_\lambda N_\lambda(T_0)\tau_\lambda \tag{60}$$

where the radiance of the atmosphere itself is neglected, and where ϵ_λ is the emissivity of the surface at wavelength λ, $N_\lambda(T_0)$ is the black-body radiance at surface temperature T_0 and wavelength λ, and τ_λ is the atmospheric transmission at λ.

The black-body radiance is derived from Planck's law [59]

$$N_\lambda(T_0) = C_1/\lambda^5[\exp(\frac{C_2}{\lambda T} - 1)] \tag{61}$$

where $C_1 = 2hc^2 = 1.19 \times 10^{-12}$ w cm^2 sr^{-1} [λ in cm],

and $C_2 = 1.4388$ cm °K.

The units of $N_\lambda(T_0)$, which expresses the radiance received at the satellite,

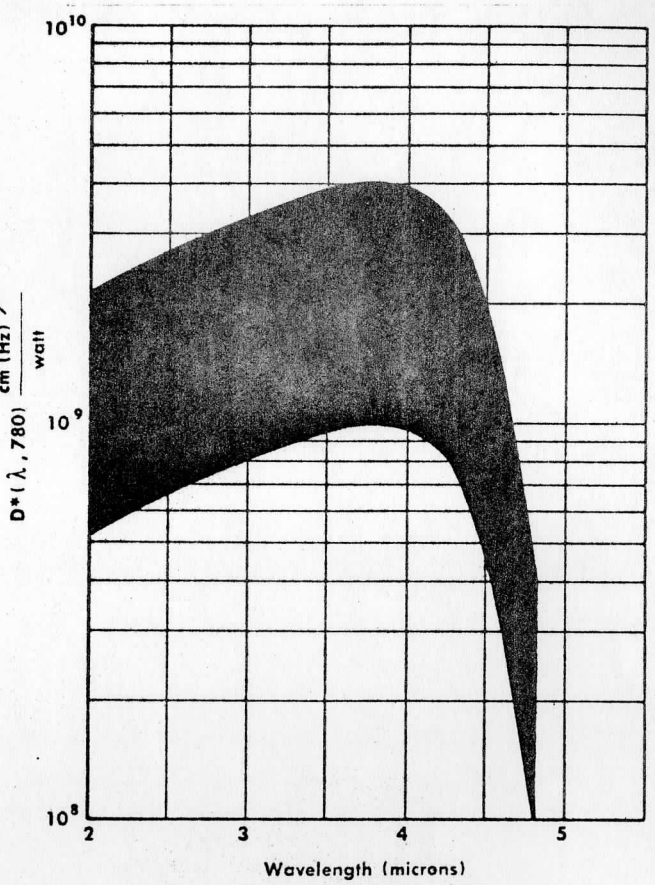

Fig. 16. Range of Spectral Detectivities for PbSe (ATO) Detectors at 295 °K.

are therefore w cm^{-3} sr^{-1} (λ in cm).

For a rough estimate, let $\epsilon_\lambda = 1$ for all wavelengths of interest.

The transmission, τ_λ, is given by the expression

$$\tau_\lambda = \exp(-K_\lambda px) \tag{62}$$

where K_λ is the absorption coefficient per unit pressure and per unit length, p is the pressure, and x is the path length. The optical path through the atmosphere in a vertical direction from the earth's surface to infinity is equivalent to a distance of approximately 5.5 km at sea level for many purposes [58]. A tabulation of K_λ values for carbon monoxide appears in [29]:

μ	K_λ(300°K) atm^{-1} cm^{-1}	cm^{-1}
4.819	.109	2075
4.761	2.05	2100
4.705	2.41	2125
4.651	1.20	2150
4.597	3.58	2175
4.545	1.47	2200

Using this table, a CO partial pressure of 10^{-7} atm (0.1 ppm estimated world wide average), a bandwidth of 150 cm^{-1} centered at 2150 cm^{-1}, and a path length of 5.5 km, the transmission is found from Eq. (62) to be 0.917. At the satellite we therefore have, from Eq. (60), approximately $E_\lambda(T_0)\Delta\lambda = 1.71 \times 10^{-4}$ w cm^{-2} sr^{-1}.

Over a range of wavelengths we can express the transmission τ by a sum over a given number of 25 cm^{-1} intervals as follows:

$$\tau = e^{-\Sigma K_\lambda px} \tag{63}$$

where K_λ is the absorption coefficient (atm^{-1} cm^{-1}) at 300°K, p is the CO partial pressure, and x = 5.5 km. The table following shows calculated ΔE values for a bandwidth of 150 cm^{-1} and selected partial pressure changes, $\Delta p/p$.

Observed Intensity Change for Given CO Partial Pressure Change

$\frac{\Delta p}{p}$	$\Sigma k_\lambda px$	τ	$\frac{\Delta E}{E}$	ΔE
0%	0.0863	0.9173	0.0000	0.0000 w cm^{-2} sr^{-1}
1%	0.0871	0.9166	0.00076	1.30×10^{-9}
10%	0.0949	0.9095	0.0085	1.46×10^{-8}
50%	0.1294	0.8786	0.0423	7.22×10^{-6}
100%	0.1726	0.8416	0.0824	1.41×10^{-5}

Following Krauss ("Performance Analysis of a Proposed High Accuracy Geostationary Sounding and Imaging System," Space Science and Engineering Center, University of Wisconsin, April 1970), we can find the detector area necessary, assuming a noise equivalent radiance, NER, equal to the signal change for a given atmospheric composition change.

$$NER = \frac{(A_d \Delta f)^{1/2}}{A_0 \alpha^2 D^* \Delta\nu \rho_\lambda} \tag{64}$$

where Δf is the reciprocal of the viewing time per rotation for a spinning instrument ($10.5/\alpha$ for the current design of an SMS satellite), A_0 is the effective aperture area (cm^2)(1200 cm^2), α is the solid angle field of view (sr), ρ_λ is the spectral response of optics (0.4μ), A_d is the detector area, and $\Delta\nu$ is the bandwidth.

The field of view is given by

$$\alpha = \frac{A_d^{1/2}}{F} \tag{65}$$

where F is the telescope's focal length (F = 122 cm. in the present case).

The change in radiation intensity due to the change in CO concentration is given by

$$\Delta E = \Delta\nu \, NER = \frac{1.11 \times 10^3}{A^{3/4} D^*} \quad . \tag{66}$$

As an example, we note that a cooled In(Sb) detector (77 °K) has a

$D^* \approx 6 \times 10^{10}$ at 4.6μ, while a Pb(Se) detector (295°K) has a $D^* \approx 1 \times 10^9$. The table below shows the required detector sizes for various values of ΔE.

Required Detector Size for CO Experiment

D^*	ΔE	$A_d^{1/2}$ (cm)
1×10^9	10^{-8}	22.0
	10^{-7}	4.82
	10^{-6}	1.07
	10^{-5}	0.23
6×10^{10}	10^{-8}	1.44
	10^{-7}	0.32
	10^{-6}	0.07
	10^{-5}	0.015

Krauss has found that by using the off-axis radiation in the primary focal plane of the SMS satellite, a 100-200 km ground resolution requiring a 2 mm square uncooled detector would be ideal. A detector of this area would provide 100 measurements per hour within 200 km of any point on earth, and would detect 30 - 40% changes per day in CO from the global average. Global detection and monitoring of carbon monoxide appears feasible.

VII. APPLICATIONS OF LASERS TO AIR POLLUTION RESEARCH

Introduction

The monochromaticity, high intensity, and directionality of laser radiation have made the laser a tool of great importance in many studies that involve the illumination of a molecular species. It is natural to ask whether techniques now available might be extended to satellite-based instrumentation designed to make measurements pertinent to the problems of air pollution. The present chapter of this report is devoted to a review of the areas in which lasers are finding a place in air pollution research, with the idea that the available power on board satellites may allow their use in the future.

At present it appears that measurements of the earth's atmosphere of direct applicability to air pollution will be most easily and fruitfully performed using the sun as a source of illumination. A laser system requires roughly a kilowatt of input power, which is about the limit of present satellite capability. Given the need for basic data in global air pollution studies that can be conveniently obtained with the sun as a source, one is prompted to postpone the advocacy of lasers for satellite-borne experiments to the future, when their special capabilities can best be used efficiently, and when a kilowatt will not so severely tax the power requirements of other experiments on board a satellite.

The place of lasers in air pollution studies may well extend to satellite experiments in the future, but at present it would appear that they will best serve to augment satellite measurements in ground-based calibration or in laboratory experiments.

Present applications of lasers in air pollution research can be classified according to the physical processes involved in light scattering. This chapter therefore takes up the techniques of resonance fluoresence, Raman

scattering, infrared absorption, Rayleigh scattering and Mie scattering in order.

Resonance Fluorescence [61, 62]

Resonance fluorescence can take place when an incident photon is absorbed by an atom or a molecule, raising it to an excited state. If one of the mechanisms for return to the ground state is a radiative process, the molecule then emits a fluorescent photon whose energy corresponds to the energy difference between the excited and the final states. The emitted photon need not be of the same wavelength as the incident photon, and in the case of molecules it very often is not. The reason for this is that there are many vibrational-rotational levels in the ground electronic state, to which the molecule can return by a radiative process, with comparable probability.

An example of the process is provided in Figure 17. An incident photon of energy $h\nu$ is absorbed by a molecule in one of the thermally populated vibrational-rotational levels of the ground state. This raises it to a vibrational-rotational level of an excited electronic state, from which it can return to a number of levels in the ground state by emitting a photon of the proper energy. The selection rules for dipole radiative processes and the Franck-Condon factor between the upper and lower energy levels govern the probability that the transition will take place between any two levels, and therefore govern the relative intensities of the fluorescence spectral lines.

It is clear that the absolute intensity of radiation in any convenient number of spectral lines can be related through experimental parameters to the molecular density, and this provides an indication of the potential usefulness of this technique to measure the density of a certain molecular species in the presence of others. Bowman [63] has, in fact, observed fluorescence from the atomic sodium layer in the atmosphere at approximately 95 km by exciting the species with a dye laser tuned to the sodium resonance line at 5896 Å. There are only approximately 10^9 sodium atoms per square cm in a column extending

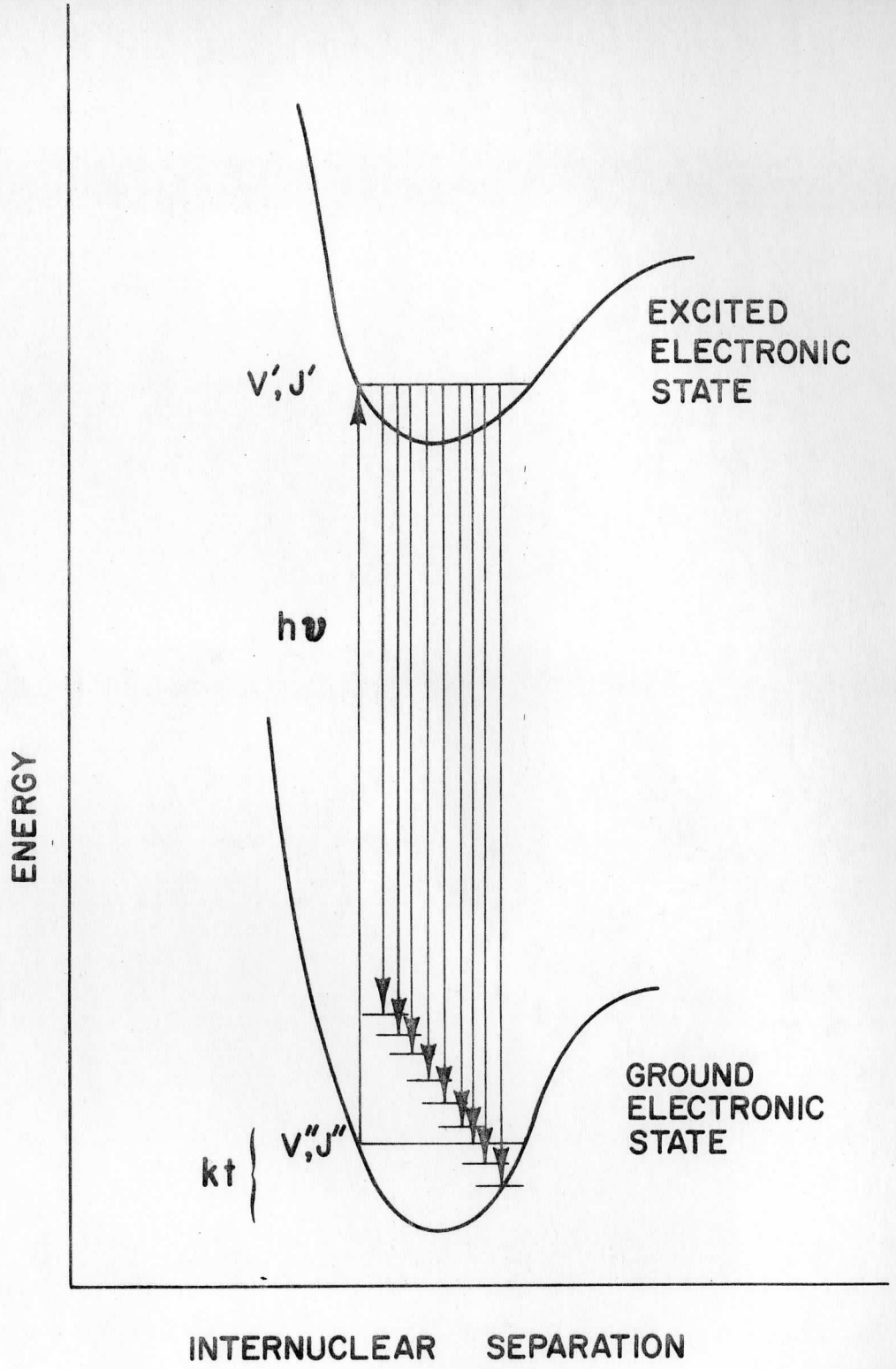

Fig. 17. An incident photon, $h\nu$, raises a molecule to an excited state. Radiative decay to a number of vibrational-rotational levels in the ground state is then possible.

through the atmosphere, which gives a feeling for the intensity available in the fluorescence technique.

The usefulness of laser-induced molecular resonance fluorescence to make remote quantitative measurements of atmospheric pollutants is not without its difficulties, and these will be discussed in a moment; but a series of recent papers has demonstrated the potential of the technique in the performance of basic research on molecular species themselves. The fluorescence spectra of the diatomic alkali molecules K_2, Na_2 and NaK [64-66] have been analyzed to obtain the spectroscopic constants of these molecules to new precision, and the technique holds promise of applicability to other molecular species as well. Figure 18 shows the fluorescence spectrum of Na_2 excited by the 4727 Å line of the argon laser as a concrete example of the principle illustrated in Figure 17.

It is worth a moment of explanation in order to understand this technique. In this case the incident laser line profile overlaps the Na_2 absorption profile for the transition between the $v'' = 1$, $J'' = 37$ level of the $X\,^1\Sigma^+$ ground state and the $v' = 9$, $J' = 38$ level of the $B\,^1\Pi$ state. Fluorescence then takes place in downward transitions to the v'' levels that have significant Franck-Condon overlap with the lower state vibrational levels, and to those lower state rotational levels that obey the dipole selection rule $\Delta J = 0, \pm 1$. [The $\Delta J = 0$ transition is not observed in this case because of an additional restriction on the symmetry of rotational levels.]

The rotational levels of each electronic state may be classified according to the behavior of the total molecular wavefunction with respect to inversion through the origin. A rotational level is called positive or negative depending on whether the parity of the total wavefunction is even or odd. For a $^1\Sigma^+$ electronic state, the diatomic molecule behaves as a simple rotor and the parity of the total wavefunction is determined solely by the parity of the rotational part. For a $^1\Pi$ electronic state the diatomic molecule behaves as a symmetric top, and for each value of J there is a positive and negative rotational level (so-called Λ doublet) of equal energy. Actually, a splitting (Λ-type doubling)

of these degenerate levels occurs because of the interaction between electronic and rotational motion. However, this splitting is so small in the case of Na_2 that its effect is negligible.

The selection rules for dipole radiation only permit positive levels to combine with negative levels and vice versa. As a consequence, when the Na_2 molecule is irradiated with monochromatic light, it is excited to either the positive or the negative Λ-type doublet of a particular upper state (v', J') level, but not to both. The resultant fluorescence spectrum consists of either P and R doublets, as in Figure 18, or single Q lines, but not P, Q, and R triplets from the same upper state (v', J') level. The net result of these restrictions is a vastly more simplified spectrum than would otherwise be the case.

Absorption spectroscopy has long been the conventional means of obtaining molecular spectra. However, this method is limited by its nature to the investigation of those ground state vibrational levels which are thermally populated. Moreover, for molecules like Na_2, which have large moments of inertia and small force constants, the absorption spectrum suffers from a superfluity of densely packed lines which cause so complex an appearance that analysis is often impeded and in some cases is altogether impossible.

On the other hand, excitation of a single isolated upper level and analysis of the subsequent fluorescence represents a complementary technique which eliminates many of the difficulties associated with absorption spectroscopy. The fluorescence spectrum is simple in appearance and can be readily resolved. Moreover, one obtains information about the high vibrational levels of the ground state. If a sufficient number of fluorescence series can be found originating from different (v', J') levels of the upper state, spectroscopic analysis of the excited state can be completed as well.

The use of laser lines as a light source to excite fluorescence is more than a mere extension of the use of metal arc lines. Because of the high intensity, directionality, and monochromaticity of the laser beam, whose wavelength can be chosen from a set of many possible laser transitions, a particular vibra-

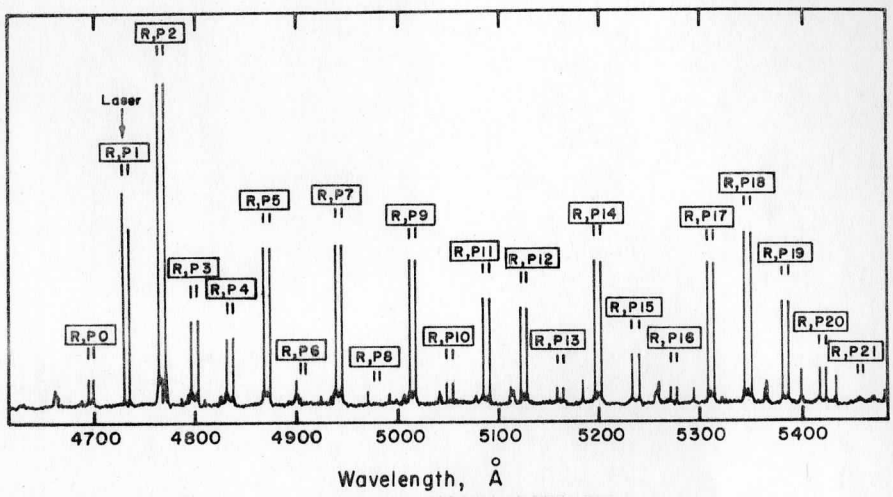

Fig. 18. Fluorescence spectrum of Na_2 excited by the argon-ion laser line $\lambda = 4727$ Å. The prominent P and R doublet fluorescence progression, ($v' = 9$, $J' = 38$) (v'', $J'' = J' \pm 1$) has been marked (P, R0), (P, R1), (P, R2), . . . , corresponding to the $v'' = 0$, $v'' = 1$, $v'' = 2, \ldots$, members of the fluorescence series. Note that this departs from the more traditional spectroscopic notation in order to designate the series in v''. The doublets correspond to P(39) and R(37).

tional-rotational level of the upper state can be appreciably populated. The resultant fluorescence is sufficiently intense that many different types of experiments, which otherwise would be extremely difficult, can be carried out with relative ease. Details of the analysis can be found in the references.

The molecule Na_2 obviously has no atmospheric significance, but the technique illustrated in its analysis may be applicable to molecules that have. Nitrogen dioxide, for example, meets the requirement that an excited electronic state lies above the ground state by an amount that corresponds to the energy of a visible photon. The NO_2 molecule fluoresces a bright orange in a cell containing the gas at a pressure of approximately 5 Torr when the 4880 Å line of the argon laser provides the illumination. It seems likely that analysis of the fluorescence spectrum will provide a better knowledge of the molecule than exists at present. Certainly this technique shows promise, then, of application to air pollution research in the laboratory.

Excited State Lifetimes

The use of fluorescence to measure molecular pollutants in the troposphere suffers from a complication. Here the pressure is high enough that the mean time between collisions is comparable with the radiative lifetime of the excited state. After absorption of a photon, therefore, within the few nano-seconds or longer that the molecule would normally exist in the excited state, a collision with another molecule can cause de-excitation by a radiationless process. The relationship between fluorescence intensity and molecular density therefore depends among other things on the radiative lifetime of the excited state.

At least two techniques that use laser induced fluorescence have recently been developed for making accurate measurements of excited state lifetimes. The first, a zero field magnetic level crossing technique, was also demonstrated on the molecule Na_2. In its "zero field" form, the molecular level crossing technique exploits the change induced by a magnetic field in the polarization characteristics of molecular fluorescence. The effect occurs be-

cause the molecular Zeeman levels are degenerate at zero field (i.e., they are "crossing in magnetic field space), and this degeneracy is removed at finite fields. The coherence of the levels at zero field therefore gives rise to a characteristic spatial distribution of each of the polarized fluorescence components, and destruction of the coherence by the magnetic field changes this spatial distribution in a detectable way. Since this is expressible in terms of the splitting of the Zeeman levels and the lifetime of the scattering system, a zero field level crossing experiment provides information about the magnetic moment of the molecule and the lifetime of the excited state.

The classical view of the phenomenon is somewhat more pictorial. In this case, one invokes the model of a molecule which undergoes Larmor precession around the direction of the magnetic field vector by reason of the molecule's possession of angular momentum and a consequent magnetic moment. At a sufficiently high magnetic field, the time to precess through a large angle, say $\pi/2$, becomes short enough that it is comparable to the lifetime of the excited state, and the polarization of the original molecular fluorescence is destroyed by the reorientation of the molecule within this time.

According to either the classical or the quantum mechanical view of level crossing spectroscopy, the geometry defined in Figure 19 allows measurement of the polarization of molecular fluorescence as a function of magnetic field,

$$P(H) = \frac{I_{II} - I_{\perp}}{I_{II} + I_{\perp}} = P(0)/(1 + 2g\tau\mu_0 H/\hbar^2) \qquad (67)$$

where $P(0)$ is the polarization at zero field, g is the Lande g-factor of the molecule, τ is the mean radiative lifetime of the excited state, μ_0 is the Bohr magneton, and H is the magnetic field. A measurement of the half-width at half maximum, $H_{1/2}$, of this Lorentzian polarization curve therefore constitues a measurement of the product $G\tau$. Since g can very often be calculated to within a percent or two with confidence, the method can provide rather precise measurements of excited state molecular lifetimes.

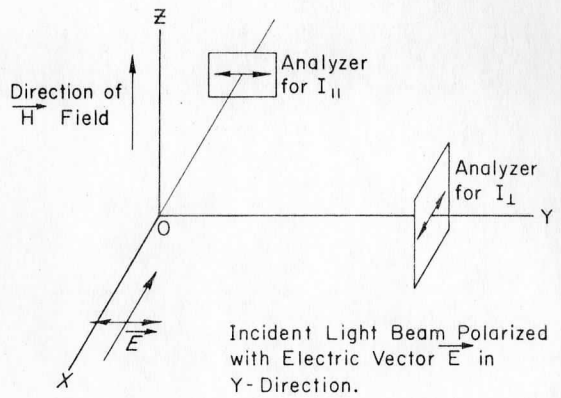

Fig. 19. Idealized experimental setup for studying the polarization of molecular fluorescence and its change with magnetic field. The light is incident along the X axis, and the molecular sample is located at the origin, O.

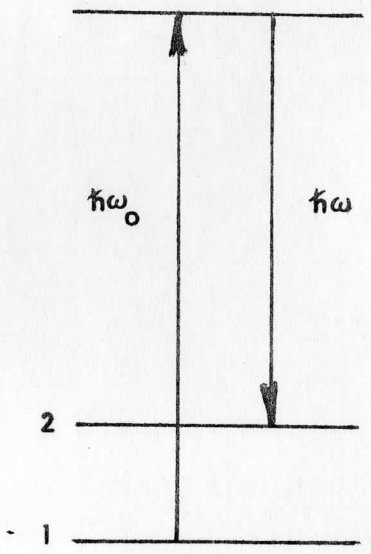

Fig. 20. Energy level diagram illustrating the Raman scattering process.

In a recent experiment, the lifetimes of several vibrational levels in the same electronic state of Na_2 were measured to demonstrate the precision of the method [67], and from these measurements the variation of transition moment with internuclear separation was calculated. Such spectroscopic data on molecules of atmospheric interest are important to the details of radiative transfer in the atmosphere.

The phase shift method for measuring lifetimes of excited states is more direct, since it does not require a calculation of the molecular g-factor to obtain the lifetime. This method, used in a form that employs laser excitation of fluorescence by Tango [68], by Baumgartner [69], and others, requires measurement of the phase shift at known frequency (the time lag) between sinusoidally modulated laser illumination and the resulting fluorescence modulation. The phase shift, ϕ, is given by

$$\phi = \text{arctangent } \omega\tau \qquad (68)$$

where $\omega/2\pi$ is the modulation frequency, and τ is the radiative lifetime under suitably careful experimental conditions. Rayleigh scattered light from the molecular species is used as the phase reference for the illuminating radiation, and light paths from the scattering cell are carefully equalized to avoid errors in optical transit times. Measurement is made at several low pressures, and these are extrapolated to zero pressure in order to avoid errors introduced by collisional quenching. This technique allows measurement of nanosecond lifetimes to approximately one percent accuracy.

Resonance fluorescence has recently been excited in NO_2 by a pulsed tunable dye laser, and the radiative lifetime of the excited state measured by noting the time constant of the exponential decay [70]. Lifetimes from 70 to 82 microseconds were measured, depending on the exciting wavelength. This kind of laboratory work paves the way for the possibility of using molecular fluorescence as a field measurement of molecular density.

Raman Scattering

The scattering of light from the viewpoint of quantum mechanics is a two-photon process involving an incident photon and a scattered photon, not necessarily of the same frequency. In the general case, that of Raman scattering [71], the difference in energy of the incident and the scattered photons is accounted for by the creation or destruction of an excitation in the scattering medium. The energy level diagram shown in Figure 20 illustrates the process in which an incident photon of energy $\hbar\omega_0$ encounters a scatterer in state 1, for example a molecule, and leaves it in state 2. The scattered photon has energy $\hbar\omega$, smaller than $\hbar\omega_0$ by an amount equal to the energy imparted to the molecule, and the difference appears in the form of 1) kinetic energy, and 2) that energy necessary to raise the molecule to state 2. This is the case of Stokes Raman scattering. The anti-Stokes case occurs when the incident photon is scattered by a molecule in an excited state, and de-excitation takes place in the scattering process. The scattered photon is then more energetic than the incident photon, and is therefore shifted toward the blue.

Rayleigh scattering can be considered as a special case of Raman scattering in which the initial and final states of the molecule are the same. The only wavelength shift of the scattered photon in this case is then due to the small exchange of kinetic energy in the scattering process, negligible in the visible region of the spectrum.

There are other special cases of Raman scattering: Brillouin scattering, in which the excitation involved is the collective linear excitation of a phonon in the scattering medium; electronic Raman scattering, in which an electronic excitation is produced in the scatterer, and several other types; but the original and more traditional kind of Raman scattering is that with which we are concerned here. This is the kind in which the excitation of a vibrational state in a molecule in the gas phase results in a shift toward the red (decreased energy) of the incident photon by an amount that corresponds to the vibrational energy of the molecular excitation.

Two useful things are immediately apparent about Raman scattering: the amount of the red shift of a scattered photon does not depend on the incident wavelength of the photon, but rather on the energy of the excitation; and, since the energy of a vibrational quantum is dependent on the normal modes of vibration of the molecule (roughly speaking, on the bond strengths between atoms in the molecule and the masses of the atoms), the amount of the red shift is peculiar to the molecular species. This means that any monochromatic source of light can be used to excite Raman spectra, and that the Raman spectra serve to identify the molecular scattering species by a unique spectral signature. The Raman spectral lines appear offset from that of the incident radiation by an amount which depends on the energy of excitation in the particular molecule at hand. Vibrational excitations in molecules typically involve energies of several hundred to several thousand wave numbers, so in the visible region of the spectrum, Raman lines are offset from the incident line by typically 100 to 1000 Angstroms. Detecting vibrational Raman lines is therefore a relatively simple process spectroscopically; a single grating instrument with moderate resolution is sufficient in most cases.

There is a disadvantage to Raman spectra. They are not intense. Typically 10^{-10} or 10^{-12} of the incident light will be Raman scattered, depending on molecular polarizability and other things, not all of them completely understood in detail. This disadvantage can be overcome, however, by using the intense monochromatic source of illumination provided by the laser. The application to air pollution detection is immediately obvious, providing the signal-to-noise ratio (SNR) for pollutant species in their expected concentration can be made satisfactory. This is possible because the intensity of the laser offsets the disadvantage of small Raman scattering cross sections.

To test the feasibility of using Raman spectra for identification of molecular pollutants, one must first calculate the Raman lines expected and make sure that they do not conflict with other molecular species in the air. Table 2 shows the offset of a Raman line from the exciting radiation, $\Delta\nu$, in cm^{-1}, for several molecular species. The data are taken from Herzberg's volumes on

the subject of molecular spectra [72, 73]. Nitrogen, oxygen, water and carbon dioxide are given first as normal constituents of air, followed by carbon monoxide and the C-H bond characteristic of hydrocarbons. For the diatomic molecules, the excitation is the stretching mode of vibration between the atomic nuclei; for the triatomic molecules H_2O and CO_2 the situation is a bit more complex, but is well explained in Herzberg [72, 73], if details are required. For the C-H bond, two modes of vibration are possible: stretching of the C-H bond, and bending of this bond with respect to the rest of the molecule. Since the rest of the molecule is much heavier than the hydrogen atom, it remains fixed relative to the hydrogen, and the energy of this bending vibration is essentially the same, 1100 cm^{-1}, for many linear hydrocarbons.

Table 2. Vibrational Raman Lines for Several Common Laser Exciting Lines

Molecule	$\Delta\nu$, cm^{-1}	λ_R for λ_e = 4880 Å	λ_R for λ_e = 5145 Å	λ_R for λ_e = 6328 Å
N_2	2331	5505	5850	7405
O_2	1555	5290	5600	7005
H_2O	3655	5910	6365	8220
CO_2	1340	5210	5520	6905
CO	2145	5460	5795	7305
C-H	1100	5160	5470	6800
C-H	3020	5705	6105	7825

Table 2 also gives the approximate wavelength of the Raman line, λ_R, in Angstroms, for three common laser exciting lines in the visible, λ_e, 4880 and 5145 Å, available with the argon laser, and 6328 Å available with the helium-neon laser.

From this table one sees the convenient spectral location of Raman lines. In fact, since the smallest $\Delta\nu$ is for the C-H bending vibration, about 280 Å, it is possible in principle to excite Raman spectra with both the 4880 and 5145 Å lines simultaneously and accept all four of the Raman lines for C-H from 5160 Å

to 6105 Å in order to provide greater sensitivity for the detection of hydrocarbons. An argon laser might be allowed to run on the three or four most intense lines and select all the Raman lines generated by these exciting lines which are appropriate to one species. One needs a short wavelength cutoff filter which eliminates all laser lines from the spectra, but allows passage of all the Raman lines.

Table 2, although abbreviated, also shows that the spectra of several species do not, in general, tend to overlap. The closest pair of Raman lines are the 5505 Å line of N_2 for λ_e = 4880 Å, and the 5520 Å line of CO_2 for λ_e = 5145 Å. The closeness of these lines would call for a spectrometer pass band of approximately 15 Å, not difficult to achieve, and even this would be appropriate only in the event one wanted to distinguish CO_2 from N_2.

Table 2 serves to illustrate the principles, but a careful and more extensive table of this kind should be drawn up using experimental data for the various atmospheric pollutants to be measured. The review of "pre-laser" Raman work by Murphy, et al. [74] provides information to supplement the earlier work compiled by Herzberg.

The intensity of Raman spectra, as well as the spectral location of the Raman lines, varies for different types of molecules. Whereas the spectral signature of a molecule serves to identify its presence, the intensity of the Raman spectra is proportional to the density of that molecule in a sample containing several gases. Using a rather simple, single grating instrument and an argon laser with an output power of approximately 1 watt, many molecular pollutants can probably be measured to a part in 10^7. With additional care, one can probably improve this by two orders of magnitude. Recent work by Schwiesow and Derr [75] is consistent with this estimate.

Although the Raman scattering intensity varies for different molecules, this can be obtained fairly well either from calculations, as demonstrated, for example, by Murphy [74], or from compilations of experimental data. In any event, one would eventually calibrate the instrument against samples of known

composition, were this technique to be used as the basis for a measurement device.

The lifetime problem present in the case of resonance fluorescence is absent in the case of Raman scattering since virtual levels are involved rather than real levels, and the scattering process therefore takes place in times of the order of 10^{-13} seconds. This is a time short compared to the mean time between collisions at atmospheric pressure, and therefore the observed Raman intensity bears a unique relation to the molecular density.

So far, Raman scattering has shown itself to be applicable to measurements of molecular air pollutants at the site of the instrument by work of Schwiesow and Derr [75], Bernstein [76] and others [77, 78], and has been extended to as far as a few kilometers by Cooney [79] and by Leonard [80], but the small value of Raman scattering cross-sections ($\sim 10^{-28}$ cm^2/ster) appears to obviate serious consideration of the technique for very remote sensing of molecular pollutants.

Recent work on the "resonance Raman" effect has shown that scattering cross-sections can be improved, perhaps by several orders of magnitude, in certain cases [81]. There is interest in this possibility, and work is being conducted to see if this is a likely candidate for increasing the signal from Raman scattering measurements. But even optimistic estimates still predict too small a signal for return from remote locations.

Infrared Absorption

The spectral region between 2 and 20 microns is rich in lines which represent molecular transitions between vibrational-rotational levels. Since many lasers also operate in this region, infrared absorption techniques are being looked into actively as a possible technique to measure atmospheric pollutants. If one can find a coincidence between a molecular absorption line and a laser line, the absorption of the laser line can be compared with the absorption of a line which does not correspond to a molecular transition in order to obtain the molecular density in the path of the beam.

Using the CO_2 and the I_2 lasers, Hanst and Morreal [82] have found the coincidences shown in Table 3. They estimate the sensitivity of their method rather conservatively to be that given in the last column of the table with a $\frac{1}{2}$ km absorption path from the laser to a retro-reflector and back.

It may be possible to extend this particular method to satellite-based techniques. One thinks of using the surface of a body of water as a reflector, or of using a retro-reflector on one of a pair of co-orbiting satellites.

Pressure broadening of the absorption lines presents a complexity to the analysis of the measurements, since the atmosphere is not at uniform pressure, but satellite measurements already conducted have shown the feasibility of measuring atmospheric pressure independently, so there appear to be no insurmountable obstacles to the use of this method for measuring several molecular pollutants. The precision to which measurement is possible will be affected by the presence of species with spectra which interfere with that of the desired species. But even this does not appear to be an obstacle which cannot be overcome by using laser lines properly located to determine the density of interfering species.

Table 3

Molecule	Laser	Laser Line	Estimated Sensitivity
CO	I_2	4.86 μ	2 ppm
NO	I_2	5.5 μ	1 ppm
SO_2	CO_2	9.08 μ	1.5 ppm
O_3	CO_2	9.52 μ	0.15 ppm

Scattering from Aerosols

Light scattering from particles of a size comparable to the wavelength of the incident light is referred to as Mie scattering. Although the theory has been developed for homogeous spherical particles, it has been applied to particles which do not fit these restrictions in an attempt to obtain information about aerosols in the atmosphere. An excellent review article by Erickson [83]

provides an up-to-date resume of the field, and provides the basis for this section of the present report.

The principle of the standard lidar (Light Detection and Ranging) technique is identical to that of the ordinary microwave radar. A pulse of energy is transmitted, the return signal from scattering is detected and its energy measured as a function of range, the range being determined by time of flight. A narrow column of the clear atmosphere at the zenith is illuminated by the pulse which usually has been passed through an optical system to obtain milliradian or less beam divergence. The light scattered back from the atmosphere is collected by a telescope, passed through a narrow-band filter, and focused on a photomultiplier tube (PMT). The geometry of the monostatic arrangement is shown in Figure 21. Due to the exponential dependence of atmospheric density upon height, the atmosphere separates into two regions from the standpoint of signal level. Below a certain height the return produces a photoelectron current and oscilloscope photography is used for data acquisition and display. Above this height the return is so weak that single photoelectron counting is used with digital pulse counting techniques and on-line digital computers for real-time data processing of pulses in a series of gated intervals corresponding to certain heights.

If the scattering is assumed to be primarily Rayleigh scattering from atmospheric molecules, then the scattered signal is proportional to the density of molecules at the scattering height. It can thus be used to measure the atmospheric density, and consequently its pressure and temperature. However, the atmosphere contains aerosols at various heights and the problem is one of distinguishing between the types of scatterers.

Rayleigh scattering of light occurs in a gas when the incident wavelength is much greater than the dimensions of the scattering particles and is different than that of any absorption line. Rayleigh theory [84] predicts the backscattering function ρ_R per molecule to be

$$\rho_R = 4\pi^2(\mu - 1)^2/n^2\lambda^4 \qquad (69)$$

where λ is the incident wavelength, n is the molecular number density, and

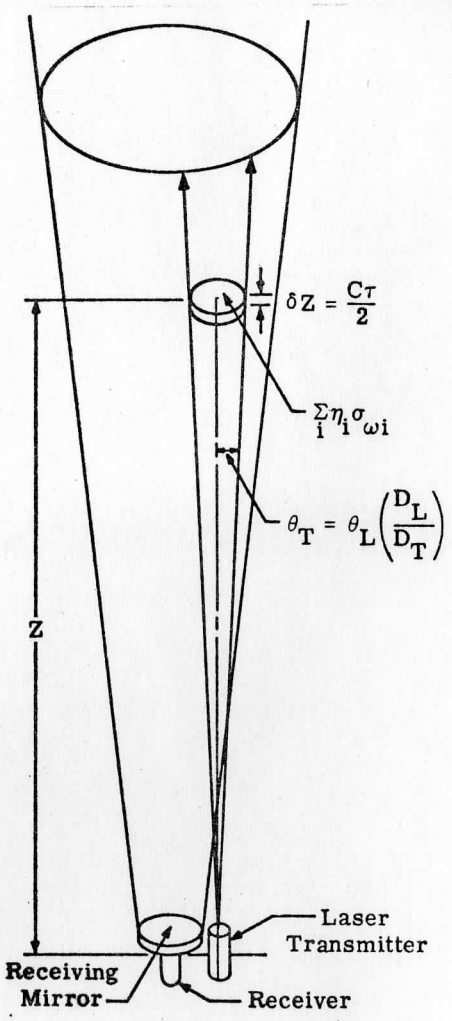

Fig. 21. Lidar Geometry (Monostatic).

μ is the refractive index of the gas. When applied to the atmosphere μ is the mean refractive index of the gas mixture. ρ_R is essentially a constant for a given wavelength up to about 90 km in the atmosphere. Dissociation of molecular oxygen occurs above this height and ρ_R begins to vary.

Atmospheric aerosols make an important contribution to the scattering from heights below 30 km and may be important for heights above 70 km. It is well known that aerosols exist over a wide range of sizes in a continuous size distribution. Stratospheric aerosols have radii up to 1 μ or more [85] and since these dimensions are of the same order as the wavelength of the incident light, simple Rayleigh theory does not apply. The theory of electromagnetic scattering by particles in this size domain is referred to as Mie theory even though Mie theory rigorously applies only to spherical particles [86]. It is not unreasonable to use the results of Mie theory to estimate the scattering from aerosols even though there is no evidence to show that aerosols are spherical with the exception of liquid droplets in the troposphere.

Using a Junge size distribution [85] for stratospheric aerosols in the Mie theory, it can be shown [87] that the volume back-scattering coefficient depends on the wavelength to the $(3-\nu)$ power where ν is a size parameter between 3 and 4 for particle radii between 0.1 and 1 μm . This wavelength dependence is very different from that of Rayleigh scattering and makes possible the measurement of the two effects by making lidar observations at different wavelengths.

The theory of scattering from aerosols in the mesosphere is more difficult because there is little knowledge of the size, shape, or composition of mesospheric particles. The scattering properties will depend on the presence of an ice coating on the particles and knowledge of this depends on the mesospheric temperature curves [88].

As lidar pulses pass through the atmosphere both scattering and absorption occur. The intensity of the return from any height depends on the total transmission losses which occur below that height. Two wavelengths are used in lidar differential absorption studies. One wavelength inside an atmospheric

absorption line is transmitted and attenuation takes place. This may be measured by comparison of the return with that scattered from the same height at a second wavelength outside the line. Attenuation as a function of height may be measured in this way and used to obtain the density profile of the atmospheric constituent causing it.

A single lidar equation describing the number of photons per pulse received from an altitude Z meters distant and detected includes a description of all the scattering examined above for a monostatic or coaxial lidar system. Assuming that the atmospheric properties do not change appreciably in the path or height layer δZ (stratified atmosphere) and that the transmitted pulse length is short compared with the time τ of the gated interval in the receiver, it can be shown that for complete beam overlap the number of photons per pulse is given by [89, 90]

$$N = N_0 A T^2 \eta \left(\sum_i n_i \rho_i / Z^2 \right) \delta Z \qquad (70)$$

where $N_0 = E_0 \lambda / hc$ is the number of photons of energy E_0 and wavelength λ in the transmitted pulse (h is Planck's constant and c is the speed of light), A is the photon collecting area of the receiver, $T = T(\lambda, Z)$ is the atmospheric transmission to the altitude Z meters distant for wavelength λ, η is the overall receiver counting efficiency, $n_i = n_i(Z)$ is the number density of scattering particles of type i at distance Z, ρ_i is the back-scattering coefficient of species i, defined as the fraction of light back-scattered per unit path length, per unit solid angle, per particle, per unit volume, and $\delta Z = c\tau/2$ is the layer thickness where τ is the time duration of the gated interval.

Several lidar systems are in operation [91-94]. Sanford has discussed various figures of merit which may be used to describe these systems [90]. Figure 22 shows Rayleigh scattering from the U. S. standard atmosphere at 45°N for a typical lidar system (solid line) and for a larger system similar to some coming into operation (dashed line). $N_0 A T^2 \eta \delta z = 4.4 \times 10^{19}$ photon m^3 for the typical case and 4.4×10^{21} photon m^3 for the larger system.

In any determination of an atmospheric profile, a large number of pulses

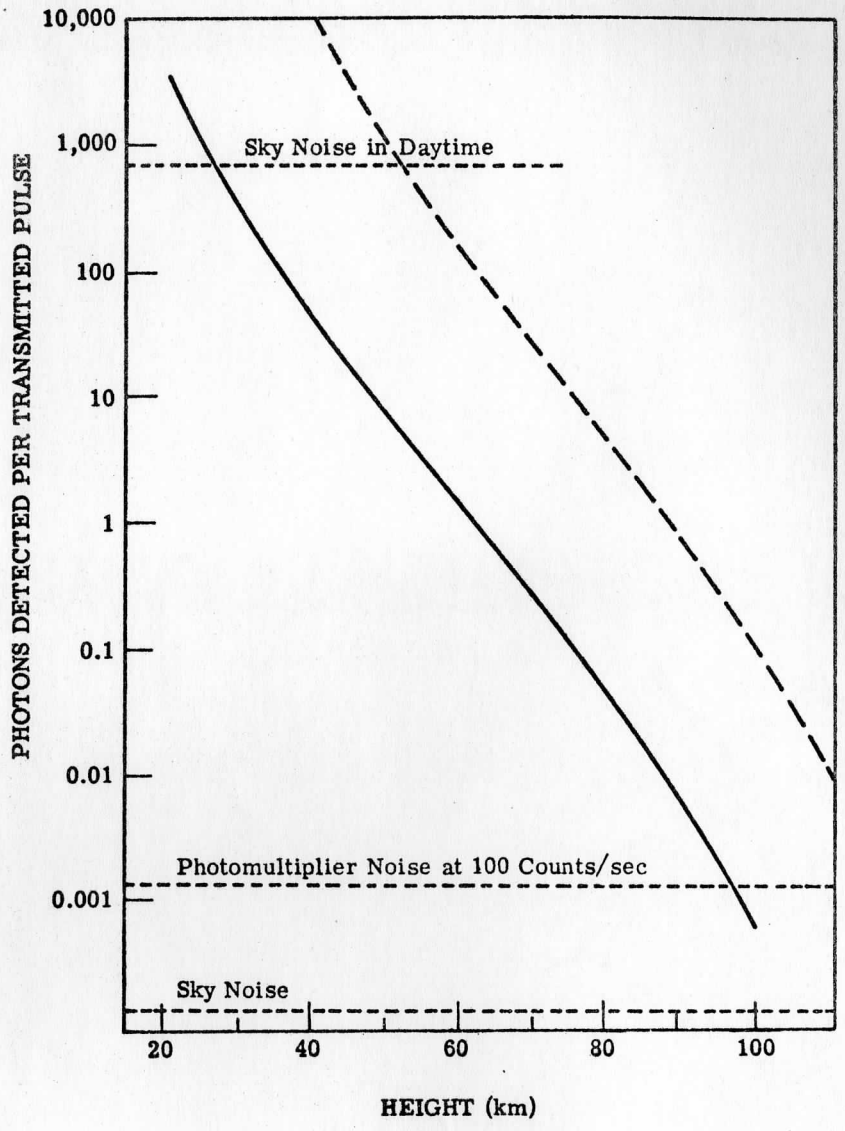

Fig. 22. Detected Photons as a Function of Scattering Altitude for Typical Lidar Systems.

is usually summed. To obtain statistical significance for high altitudes, a very large number of pulses are normally required. In addition to statistical fluctuations, there are errors traceable to noise in the system which must be accounted for. This noise has two basic sources: thermal noise from the PMT, and unwanted photons from airglow and other sky background. Spurious effects caused by laser fluorescence [95] or overloading of the PMT may also occur but these can be eliminated by careful experimental techniques (e.g., high speed shutters). The sky noise shown in Figure 22 was calculated by assuming it is entirely due to airglow, that the receiver area is $0.25 m^2$, has a 10 Å filter, and field of view of one mrad. Scattered light from urban areas or other sources can be removed only by a careful choice of site. Multiple scattering contributes returns from the close atmosphere before beam overlap occurs, but otherwise is not a significant source of noise below 150 km [96]. The daytime sky noise is also shown in Figure 22. It can be seen that even with use of polarized filters and narrower fields of view, it is nearly impossible to obtain useful returns from the highest altitudes during the daytime.

The reliability of these systems is not yet great but will improve with experience in their use. Photomultiplier tubes with 10-15% quantum efficiency at 6943 Å, 2-4 Å filters with 60-80% transmission at 6943 Å, fast digital electronics in the receivers for increased height resolution, and more powerful lasers with higher pulse rates are already operating in the field. Accuracy will only improve as the square root of the improvement in performance, but reasonably large improvement is being made.

Some preliminary measurements have been made using two wavelengths, ruby and a frequency-doubled ruby laser [97], and using three wavelengths [98]: neodymium (1.06 μm), frequency-doubled ruby (.3472 μm), and ruby (.6943 μm). Such measurements offer a possibility of separating the scattering due to molecules and to aerosols, because of different wavelength dependence for these species.

The data from a long series of measurements have been compared with

various meteorological parameters and very little correlation has been found [99]. An average profile of the ratio of total to aerosol scattering shows a maximum of 1.9 at about 17 km. The r. m. s. deviation of this ratio is only 0. 3, indicating that the layer is remarkably constant. When auto-correlation coefficients were calculated the correlation was found to drop to zero in about 5 days. No marked seasonal variation was observed. Attempts to correlate the aerosol return with wind velocity and direction and with the height of the tropopause all gave negative results. Similar attempts have been made by Kent and Wright [97] also with negative results.

Observations of scattering from heights up to 30 km during daylight have been made [89]. This is made possible by the very strong returns obtained from this region. It is clear that 24-hour observations of the aerosol layer are possible under suitable weather conditions.

The problem of whether it is possible to observe scattering of a lidar beam by an aerosol layer at heights above 60 km is one that has caused considerable controversy during the past five years. The earliest lidar observations very clearly had spurious sources of noise which were then unknown, and which only became obvious later. In the absence of obvious other causes, any excess photon count, over that expected from Rayleigh scattering, is attributed to scattering from aerosols. Recent experiments have succeeded in reducing or eliminating these spurious sources of noise with some reduction in the strength of the returns from the apparent aerosol layers.

Of all the techniques mentioned, it appears that absorption is the most likely candidate for satellite based measurements. The greatest signal-to-noise ratio is attainable with this technique at distances characterized by satellite altitudes because one does not suffer from the $1/R^2$ loss of signal as in the scattering techniques.

VIII. REFERENCES

1. Berkner, L. V. and L. C. Marshall, "The Rise and Stability of the Earth's Atmosphere," Brookhaven Lecture Series #64, March 8, 1967.

2. Johnson, F. S., "Atmospheric Oxygen and Carbon Dioxide," Southwest Center for Advanced Studies, April 1969.

3. Edlen, B., "The Dispersion of Standard Air," J. Opt. Soc. Amer. 43, 339 (1953).

4. van de Hulst, H. C., Light Scattering by Small Particles. Wiley, 1957.

5. Blattner, W. G., Calculations of Atmospheric Attenuation Parameters and Angular Scattering Data for Light Scattering in Model Atmospheres. Radian Research Associates Report RRA T 702, 1970.

6. Junge, C. E., Air Chemistry and Radioactivity. International Geophysics Series 4, Academic Press, 1963.

7. Quenzel, H., "Determination of Size Distribution of Atmospheric Aerosol Particles from Spectral Solar Radiation Measurements," J. Geophys. Res. 75, 2915 (1970).

8. Yamamoto, G. and M. Tanaka, "Determination of Aerosol Size Distribution from Spectral Attenuation Measurements," Appl. Opt. 8, 447 (1969).

9. Bullrich, K. R. Eiden, R. Jeinicke and W. Nowak, "Solar Radiation Extinction, Sky Radiation, Skylight Polarization and Aerosol Particle Total Number and Size Distribution on the Island Maui (Hawaii)," Pure and Appl. Geophys. 69, 280 (1968).

10. Bach, W., Solar Radiation and Atmospheric Turbidity, Scientific Report, Kettering Lab., Univ. of Cincinnati, Ohio, Oct. 1969.

11. Volz, F. E., Spectral Skylight and Solar Radiance Measurements in the Caribbean Maritime Aerosol and Sahara Dust. Paper presented at the Spring Meeting of the Optical Society of America, Washington, D. C., 1970.

12. Sekera, Z., "Polarization of Skylight," Handbuch der Geophysik, Vol. 2, Springer-Verlag, Berlin. 1957.